*Published in : Journal of Constructional Steel Research (2022), vol. 189, 107099*
*DOI: 10.1016/j.jcsr.2021.107099*
*Status : Postprint (Author's version)*

# Analytical model for the panel zone resistance in welded steel beam-to-column joints

Adrien Corman*, Jean-François Demonceau*, Jean-Pierre Jaspart*

* *University of Liège, Belgium*

**Keywords :** Steel joints ; Panel zone ; Column web panel in shear ; Analytical model ; FE analysis

**Abstract**

This article addresses the problem of prediction of the plastic shear resistance of the panel zone (PZ) in welded steel beam-to-column joints under monotonic loading. As a first step, an extensive review of existing analytical models is proposed. The capabilities of the latter are then assessed through comparisons against available experimental data. These comparisons reveal that none of them is able to accurately capture all the complex phenomena governing the plastic shear resistance of the PZ. Therefore, a new analytical model has been developed based on the extensive use of finite element (FE) analysis. This approach includes the development and validation of a FE model within the Abaqus© environment and the use of the so-validated model in order to perform a parametric study on (non-)axially loaded (un-)stiffened exterior and interior joints. This parametric study helped to gain a better understanding of the actual stress distributions within the PZ. Based on these observations, a new analytical model is proposed and validated against the numerical results. This model proves to work well and to outperform existing analytical models by providing a more coherent estimation of the plastic shear resistance of the PZ.

## 1. Introduction

Structural joints are recognized as key elements in the design of steel and steel-concrete composite structures as they are required to connect together the structural elements (i.e. beams and columns) and to transfer internal forces (i.e. shear forces *V*, axial forces *N* and bending moments *M*) between the elements. Therefore, their behaviour must be mastered and fully understood.

In typical steel frame structures, two main types of major axis beam-to-column joints may be encountered, namely interior joints (i.e. double-sided joints) and exterior joints (i.e. single-sided joints). These two joint configurations are depicted in Fig. 1 in the most general loading case (subscripts B and C stand for Beam and Column respectively; subscripts T, R, B, L stand for Top, Right, Bottom and Left respectively). They may be divided into two main parts [1]:

*Published in : Journal of Constructional Steel Research (2022), vol. 189, 107099*
*DOI: 10.1016/j.jcsr.2021.107099*
*Status : Postprint (Author's version)*

- The panel zone (PZ) which consists of the column web panel (CWP) as well as of the so-called surrounding elements (SE), i.e. the column flanges, the root fillets and the possible transverse column web stiffeners, aligned with the beam flanges.
- The left or (and) right connection(s), concentrated at the beam end/column interface, and which is (are) made of the connecting elements (e.g. bolts, endplates…) as well as of the tensioned and compressed "load-introduction" parts of the column web.

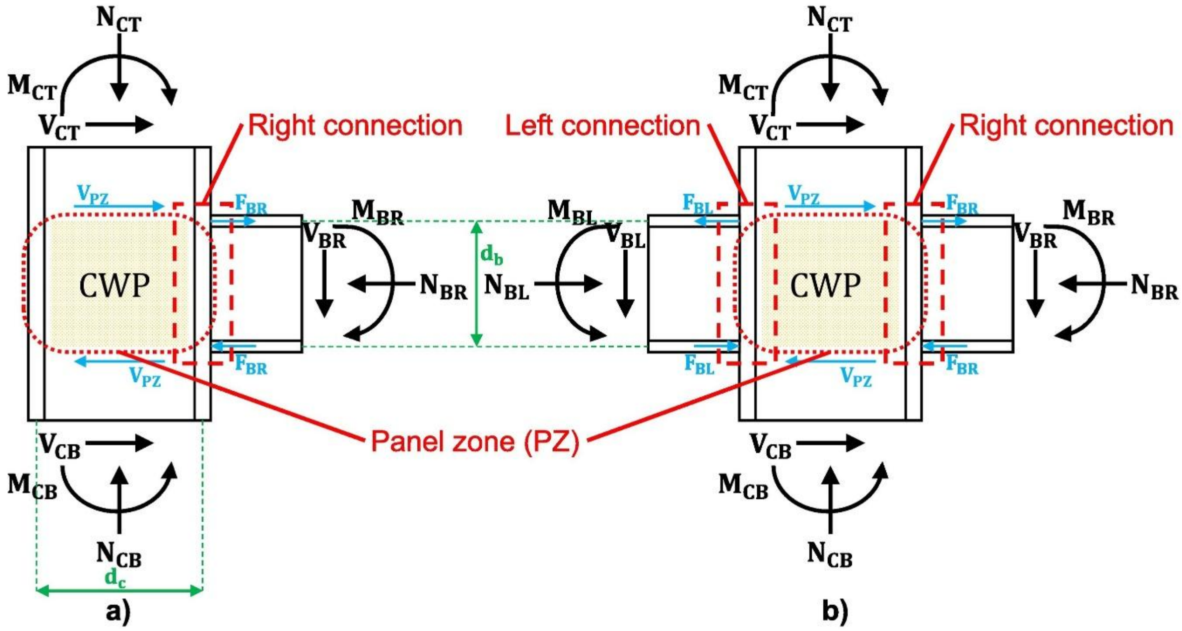


**Fig. 1.** Welded joints: (a) exterior and (b) interior configurations (adapted from [1]).

Under the loads applied to the joints, the PZ exhibits complex states of stress and strain. This is shown in Fig. 2 for exterior joints in which beams transfer bending moments and shear forces only (i.e. $N_{BR} = 0$ in Fig. 2). The state of stress is characterized by the combination of the three following stress components [[1], [2], [3], [4]]:

- shear stresses ($\tau$), coming from the equivalent shear force $V_{PZ}$, which may be evaluated with Eq. (1), $\beta$ being the transformation parameter and $d_b$ the lever arm between the tension and compression centres (assumed equal to $h_b - t_{fb}$ for welded joints);
- vertical normal stresses ($\sigma_{n,\,N-M}$), coming from the $N_C$ axial load ($\sigma_{n,\,N}$) and the $M_C$ bending moment ($\sigma_{n,\,M}$) in the column;
- horizontal normal stresses ($\sigma_i$), coming from the couple of tensile and compressive load-introduction forces $F_{BR}$, statically equivalent to the beam moment $M_{BR}$ and acting at mid-depth of the beam flanges.

$$V_{PZ} = \frac{M_{BR}-M_{BL}}{d_b} - \frac{V_{CB}-V_{CT}}{2} = \beta_R \cdot F_{BR} = \beta_R \cdot \frac{M_{BR}}{d_b} \quad (1)$$

Published in : Journal of Constructional Steel Research (2022), vol. 189, 107099
DOI: 10.1016/j.jcsr.2021.107099
Status : Postprint (Author's version)

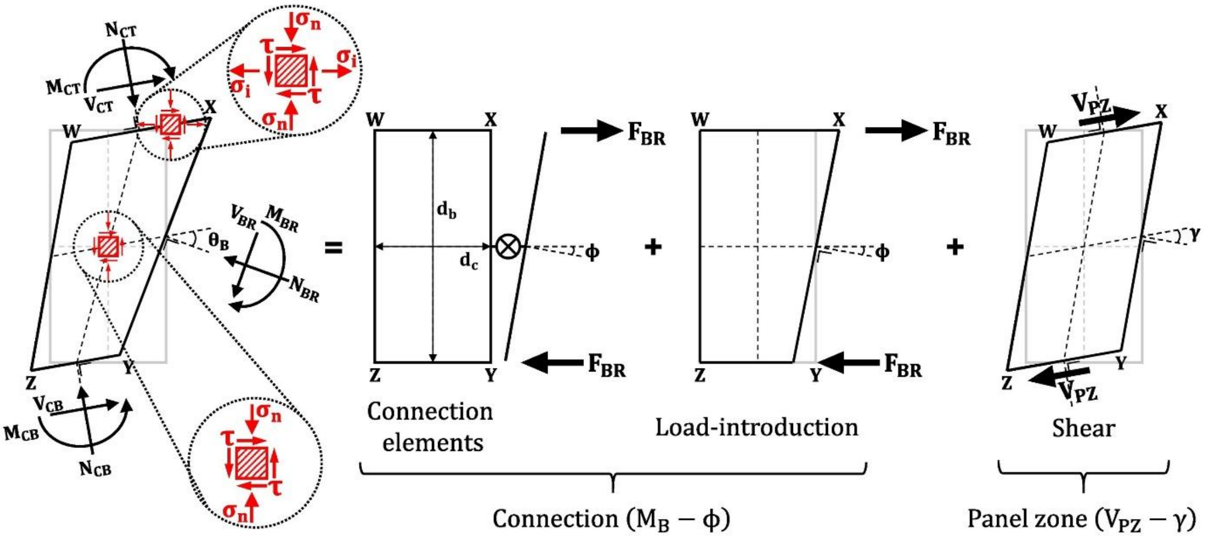


**Fig. 2.** Illustration of the state of stress and of the sources of deformability in an exterior joint (adapted from [2]).

The joint deformability arises from two different sources [1,2,5]:

- The first contribution comes from the connection, and consists of the deformation of the connecting elements (e.g. bolts, endplates…) as well as of the transverse shortening and elongation of the column web, under the couple of tensile and compressive forces $F_{BR}$. This results in a relative rotation $\Phi$ between the beam and column axes, which makes possible the derivation of a first deformation curve $M_B - \Phi$ characterizing the rotational response of the connection.

- The second contribution comes from the shear deformation of the PZ. This results in a relative rotation $\gamma$ between the beam and column axes, thus leading to a second deformation curve $V_{PZ} - \gamma$ characterizing the rotational response of the PZ. In view of a simplified modelling of the joints for structural analysis, it is sometimes suggested to substitute the $V_{PZ} - \gamma$ curve by a $M_{BR} - \gamma$ curve through the use of the so-called transformation parameter $\beta_R$ defined by Eq. (1) for the right connection, see [1].

This article focuses on the contribution of the PZ only, which turns out to govern the joint response in a significant number of situations under static loads, but even more so under seismic loading conditions [5]. More precisely, this article proposes a new analytical model for the prediction of the plastic shear resistance $V_{PZ,\,Rk}$ of the PZ. To this aim, a scientifically-based methodology has been used which consists of (i) a literature review of the most referenced scientific models (Section 2), (ii) a discussion of the strengths and weaknesses of these models through comparisons against experimental results (Section 3), (iii) the development and validation of a sophisticated finite element model (Section 4.1), (iv) the development of an extensive parametric study in order to highlight the key parameters governing the plastic shear resistance of the PZ (4.2 Parametric study, 4.3 FE results and discussion), (v) the development and validation of a new complex analytical formulation for scientific purposes, which encompasses all the so-identified key parameters (Sections 5) and (vi) the simplification of this complex model in view of its possible integration in

*Published in : Journal of Constructional Steel Research (2022), vol. 189, 107099*
*DOI: 10.1016/j.jcsr.2021.107099*
*Status : Postprint (Author's version)*

design codes (Section 6). At the end, the proposed analytical model proves to work well and to outperform existing analytical models by providing a more coherent and physically founded estimation of the plastic shear resistance of the PZ.

The scope of this article was limited to welded joints under monotonic loading only, so as to avoid the occurrence of any other failure mode in the connecting elements (i.e. bolts in tension, endplates in bending…) [5]. In addition, fillet welds were assumed to be sufficiently resistant (i.e. there is no premature failure of the welds) and the PZ dimensions were chosen to prevent the occurrence of any premature local yielding within the compressed or tensile zones of the CWP, prior to the shear yielding of the PZ.

Two types of joint configurations have been considered in the present article, namely exterior and interior joints, see Fig. 3 and Fig. 4 respectively. These joints are loaded in such a way that the PZ becomes the governing component of the joint response. This particular loading is illustrated in Fig. 3(a) and Fig. 4(a) for exterior and interior joints, respectively. Columns are subjected to an axial force *N* coming from the gravity loads, but also to shear forces and bending moments resulting from the horizontal reactions *R*. Beams transfer bending moments and shear forces only, coming from the applied external load *P*. No horizontal axial force is transferred by the beams. This kind of anti-symmetrical loading could be caused by either wind or earthquake (or even gravity loads in the case of exterior joints) and generates significant shear in the joint, especially in the PZ, as shown in the M-N-V diagrams in Fig. 3(b) and Fig. 4(b).

*Published in : Journal of Constructional Steel Research (2022), vol. 189, 107099*
*DOI: 10.1016/j.jcsr.2021.107099*
*Status : Postprint (Author's version)*

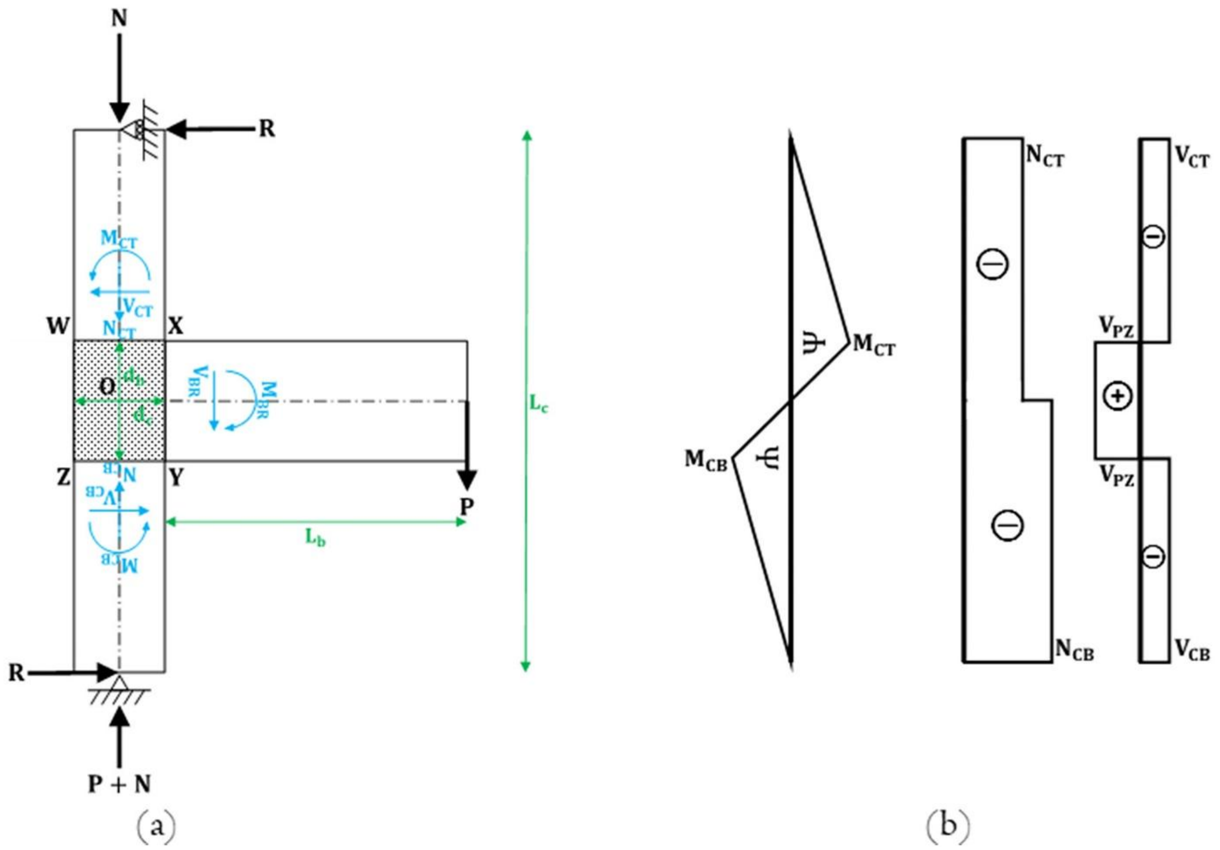


**Fig. 3.** Exterior joint: (a) loading conditions maximizing shear in the PZ and (b) resulting M-N-V diagrams in the column.

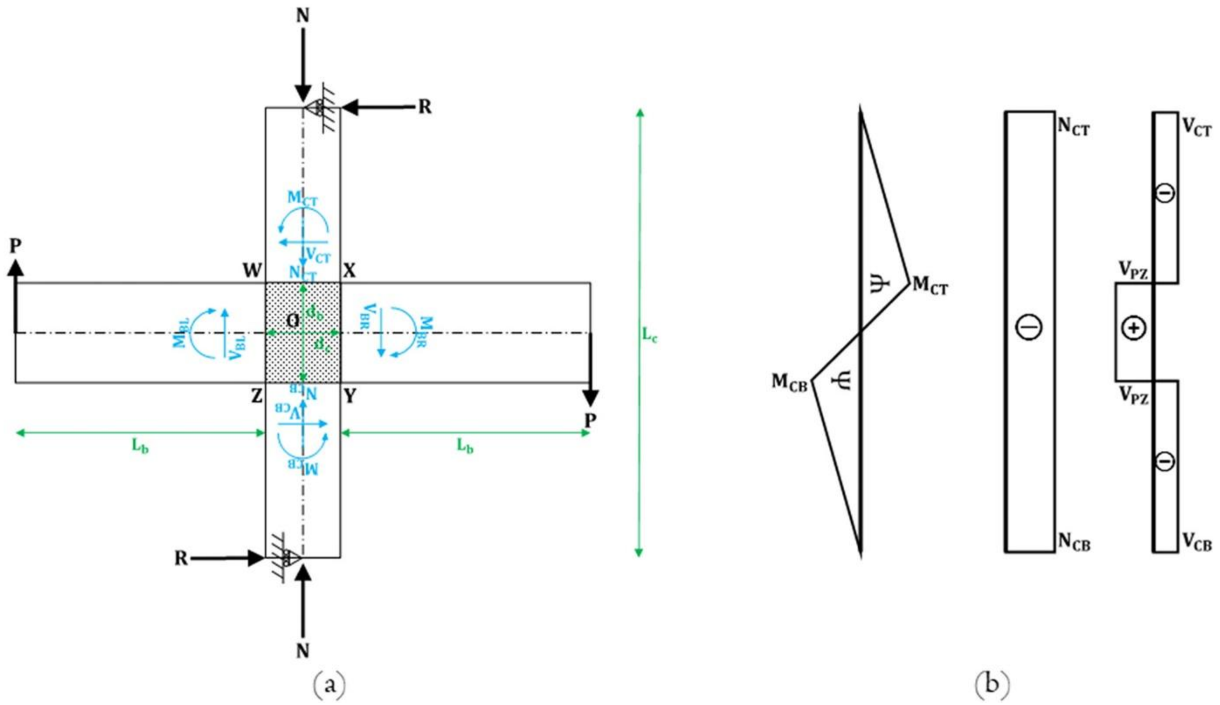


**Fig. 4.** Interior joint: (a) loading conditions maximizing shear in the PZ and (b) resulting M-N-V diagrams in the column.

*Published in : Journal of Constructional Steel Research (2022), vol. 189, 107099*
*DOI: 10.1016/j.jcsr.2021.107099*
*Status : Postprint (Author's version)*

In Fig. 3(b) and Fig. 4(b), a uniform shear distribution may be observed within the PZ. This is equivalent to saying that the beam moment $M_{BR}$ (resp. $M_{BL}$) is transferred to the PZ by the couple of equal but opposite forces $F_{BR}$ (resp. $F_{BL}$), acting at mid-depth of the beam flanges and statically equivalent to the beam moment $M_{BR}$ (resp. $M_{BL}$), see Fig. 1. This assumption seems reasonable as most of the beam moment is carried by the flanges in typical I-shaped beams [3]. Regarding the support conditions, both joint configurations are simply supported, which is similar to assuming that the point of contraflexure of the bending moment diagram occurs at the column mid-height [6].

# 2. Literature review of existing models

## 2.1. COMPLEX MECHANICAL MODELS

The behaviour of the PZ has been studied for more than 50 years by a significant number of researchers. These research efforts have led to the proposal of multiple multi-linear mechanical models, which aim at predicting the shear behaviour of the PZ. A non-exhaustive sample of these models is given in Table 1 in terms of the plastic shear resistance of the PZ ($V_{PZ,\ Rk}$) only (i.e. assumption of rigid-plastic models), this parameter being the one of interest in the present article. This sample includes the models of Fielding (1971, [3]), Krawinkler (1978, [7]), Wang (1988, [8]), Jaspart (1991, [9]), Lin (2000, [10]), Engelhardt (2002, [11]) and more recently the models of Kim (2015, [12]) and Skiadopoulos (2021, [13]).

**Table 1.** Literature review of existing analytical models for $V_{y,\ Rk}$ and $\Delta V_{y,\ Rk}$.

| **Authors** | $V_{y,Rk}$ | $\Delta V_{y,Rk}$ | **Parameters** | | | | | |
|---|---|---|---|---|---|---|---|---|
| | | | $A_{VC}$ | $d_c$ | $d_b$ | $\chi_N$ | $\Delta\chi_N$ | $\chi_{pp}$ |
| Fielding (1971) | $A_{VC} \cdot \tau_y \cdot \chi_N \cdot \chi_{pp}$ | / | $d_c \cdot t_{wc}$ | $h_c - t_{fc}$ | $h_b - t_{fb}$ | $\sqrt{1-n^2}$ | / | 1 |
| Krawinkler (1978) | $A_{VC} \cdot \tau_y \cdot \chi_N \cdot \chi_{pp}$ | $7.2 \cdot \frac{M_{pl,fc}}{d_b} \cdot \Delta\chi_N$ | $d_c \cdot t_{wc}$ | $0.95 \cdot h_c$ | $0.95 \cdot h_b$ | $\sqrt{1-n^2}$ | $\sqrt{1-n^2}$ | 1 |
| Wang (1988) | $A_{VC} \cdot \tau_y \cdot \chi_N \cdot \chi_{pp}$ | $4 \cdot \frac{M_{pl,fc}}{d_b} \cdot \Delta\chi_N$ | $d_c \cdot t_{wc}$ | $h_c - 2 \cdot t_{fc}$ | $h_b - t_{fb}$ | $\sqrt{1-n^2}$ | $\sqrt{1-n^2}$ | 1 |
| Jaspart (1991) | $A_{VC} \cdot \tau_y \cdot \chi_N \cdot \chi_{pp}$ | $4 \cdot \frac{M_{pl,fc}}{d_b} \cdot \Delta\chi_N$ | $A_{VC,\ EC3}$ | $h_c - t_{fc}$ | $h_b - t_{fb}$ | 0.9 | 1 | 1 |

Published in : Journal of Constructional Steel Research (2022), vol. 189, 107099
DOI: 10.1016/j.jcsr.2021.107099
Status : Postprint (Author's version)

| | | | | | | | | |
|---|---|---|---|---|---|---|---|---|
| Lin (2000) | $A_{VC} \cdot \tau_y \cdot \chi_N \cdot \chi_{pp}$ | $51.2 \cdot \frac{M_{pl,fc}}{d_b} \cdot \frac{t_{cf}}{d_b} \cdot \Delta\chi_N$ | $d_c \cdot t_{wc}$ | $h_c - 2.3 \cdot t_{wc}$ | $h_b$ | $\sqrt{1-n^2}$ | $\sqrt{1-n^2}$ | 1.4 |
| Engelhardt (2002) | $A_{VC} \cdot \tau_y \cdot \chi_N \cdot \chi_{pp}$ | $4 \cdot \frac{M_{pl,fc}}{d_b} \cdot \Delta\chi_N$ | $d_c \cdot t_{wc}$ | $h_c$ | $h_b - t_{fb}$ | $\sqrt{1-n^2}$ | $1 - n^2$ | 1 |
| Kim (2015) | $A_{VC} \cdot \tau_y \cdot \chi_N \cdot \chi_{pp}$ | $4 \cdot \frac{M_{pl,fc}}{d_b} \cdot \Delta\chi_N$ | $d_c \cdot t_{wc}$ | $0.95 \cdot h_c$ | $0.95 \cdot h_b$ | 1 | $1 - \frac{1}{4} \cdot n_{fc}^2$ | $0.97 + 0.009 \cdot \left(\alpha + \frac{3.45}{\alpha}\right) \cdot \Delta\chi_N$ |
| Skiadopoulos (2021) | $A_{VC} \cdot \tau_y \cdot \chi_N \cdot \chi_{pp}$ | $2 \cdot a_{eff} \cdot A_{fc}^* \cdot \tau_y \cdot \Delta\chi_N$ | $d_c \cdot t_{wc}$ | $h_c - t_{fc}$ | $h_b$ | $\sqrt{1-n^2}$ | $\sqrt{1-n^2}$ | 1.1 |

Notes: *$n = N_C/N_{pl,c}$ where $N_{pl,c}$ is the column axial strength; $n_{fc} = N_C/N_{pl,fc}$ where $N_{pl,fc}$ is the column flange axial strength; $\alpha = h_b/t_{fc}$;$A_{VC,EC3}$ see EN 1993-1-1* [14]; *$A_{fc}^* = (b_c - t_{wc}) \cdot t_{fc}$; $a_{eff}$ see* [13]

As regards the plastic shear resistance of the PZ ($V_{PZ,Rk}$), it is expressed by all the authors as the sum of two independent contributions, as given by Eq. (2). The first contribution ($V_{y,Rk}$) accounts for the plastic shear resistance of the CWP. The second contribution ($\Delta V_{y,Rk}$) accounts for the beneficial effect provided by the SE before large plastic rotations develop.

$$V_{PZ,Rk} = V_{y,Rk} + \Delta V_{y,Rk} = V_{y,Rk} \cdot \Psi \quad (2)$$

where:

$$\Psi = 1 + \frac{\Delta V_{y,Rk}}{V_{y,Rk}} \text{:flange contribution factor(FCF)}$$

For the derivation of $V_{y,Rk}$ (see Table 1), all the models assume a uniform shear distribution within the CWP and they all neglect the $\tau - \sigma_i$ interaction, the load-introduction phenomenon being assumed to be a localized phenomenon and hence not affecting $V_{y,Rk}$. However, they differ from each other according to the effective shear area $A_{VC}$ which is considered. Some researchers also account for the initiation of strain-hardening in the CWP, which is expressed by means of a strain-hardening (post-plastic) coefficient $\chi_{pp}$ different from 1.0 in Table 1.

For the derivation of $\Delta V_{y,Rk}$ (see Table 1), Wang, Jaspart, Engelhardt and Kim assume the formation of four plastic hinges in the column flanges, at the level of the beam flanges. However, Jaspart allows accounting for this beneficial frame action in the presence of transverse column web stiffeners only. Krawinkler and Lin propose empirical formulae for $\Delta V_{y,Rk}$ on the basis of experimental and numerical results. In the model of Skiadopoulos, the formula for $\Delta V_{y,Rk}$ is based on the integration of the shear stress profile in the column flanges, see [13]. Finally, Fielding does not propose any formula for $\Delta V_{y,Rk}$.

Regarding the axial load $N_C$ in the column, it is taken into account in the different models by means of two reduction factors, namely $\chi_N$ and $\Delta\chi_N$, which affect both contributions $V_{y,Rk}$ and $\Delta V_{y,Rk}$

*Published in : Journal of Constructional Steel Research (2022), vol. 189, 107099*
*DOI: 10.1016/j.jcsr.2021.107099*
*Status : Postprint (Author's version)*

respectively. In the models of Fielding, Krawinkler, Wang, Lin and Skiadopoulos, a uniform $\sigma_{n,N}$ stress distribution is assumed within the column cross-section. Therefore, $\chi_N$ and $\Delta\chi_N$ are derived based on the application of the Von Mises criterion. The same assumption is made by Engelhardt regarding the $\sigma_{n,N}$ stress distribution, but $\Delta\chi_N$ is here derived based on the M-N interaction criterion in a rectangular cross-section. Kim assumes that $N_C$ is carried by the column flanges only. Thus, he uses the same M-N interaction criterion as Engelhardt for the derivation of $\Delta\chi_N$ while assuming $\chi_N$ equal to 1.0. In his model, Jaspart accounts for the $\sigma_{n,N}$ stresses coming from the difference between the $N_{CT}$ and $N_{CB}$ axial loads in the column and for the $\sigma_{n,M}$ stresses coming from the maximum $M_{CT}$ or $M_{CB}$ bending moment in the column. The former are assumed to be uniformly distributed over the column cross-section while the latter, which are neglected by all other researchers, are assumed to be uniformly distributed over the flanges only. The application of the Von Mises criterion at the intersection between the CWP and the flanges, where the $\sigma_{n,N-M}$ stresses are maximum, provides an estimation of $\chi_N$. This value has been safely approximated to 0.9 by Jaspart, while $\Delta\chi_N$ has been kept equal to 1.0. More information on the different models can be found in the given references.

## 2.2. DESIGN PROVISIONS FOR PANEL ZONE

Some of the complex analytical models presented here above have been included in modern design codes, providing some slight adjustments. The cases of the European and American design codes [15,16] are reviewed in 2.2.1 European design code, 2.2.2 American design code, respectively.

### 2.2.1. EUROPEAN DESIGN CODE

In the part 1–8 of Eurocode 3 (EN 1993-1-8, [15]), which is dedicated to the design of steel joints, the model of Jaspart has been adopted for the evaluation of the plastic shear resistance ($V_{PZ,Rk,EU}$) of the PZ. Therefore, reference can be made to Eq. (2) and Table 1, leading to Eq. (3):

$$V_{PZ,Rk,EU} = V_{y,Rk,EU} \cdot \Psi_{EU} = A_{VC} \cdot \tau_y \cdot \chi_N \cdot \chi_{pp} \cdot \Psi_{EU} \quad (3)$$

with the following value for the FCF:

$$\Psi_{EU} = 1 + \frac{\sqrt{3} \cdot b_c \cdot t_{fc}^2}{A_{VC} \cdot d_b \cdot \chi_{pp}} \cdot \frac{\Delta\chi_N}{\chi_N} \quad (4)$$

All the parameters in Eq. (3) and Eq. (4) are similar to the ones defined in Table 1 for the model of Jaspart. As a reminder, in Eq. (3), the FCF can be accounted for in the presence of transverse column web stiffeners only.

### 2.2.2. AMERICAN DESIGN CODE

Similarly, the model of Krawinkler has been adopted by the American Institute of Steel Construction (AISC) for the evaluation of the plastic shear resistance ($V_{PZ,Rk,US}$) of the PZ. Therefore, reference can be made, here again, to Eq. (2) and Table 1, leading to Eq. (5):

$$V_{PZ,Rk,US} = V_{y,Rk,US} \cdot \Psi_{US} = A_{VC} \cdot \tau_y \cdot \chi_N \cdot \chi_{pp} \cdot \Psi_{US} \quad (5)$$

*Published in : Journal of Constructional Steel Research (2022), vol. 189, 107099*
*DOI: 10.1016/j.jcsr.2021.107099*
*Status : Postprint (Author's version)*

The parameters used in Eq. (5) are given in Table 2, depending on whether the additional strength ($\Delta V_{y,Rk,US}$) provided by the SE may be accounted for or not in the design phase. From Table 2, it can be seen that the reduction factor $\chi_N$ accounting for the $\tau - \sigma_{n,N}$ interaction in the CWP is different from the one proposed by Krawinkler. In addition, for the derivation of the shear area $A_{VC}$, the AISC suggests to use $d_c = h_c$ instead of the value $d_c = 0.95 \cdot h_c$ recommended by Krawinkler.

**Table 2.** Definition of the parameters used in Eq. (5).

| | **$\Delta V_{y,Rk,US}$ not allowed** | **$\Delta V_{y,Rk,US}$ allowed** |
|---|---|---|
| **$\Psi_{US}$** | $1$ | $1 + \frac{3 \cdot b_c \cdot t_{fc}^2}{A_{VC} \cdot d_b \cdot \chi_{pp}} \cdot \frac{\Delta\chi_N}{\chi_N}$ |
| **$\chi_N$** | $\begin{cases} 1 & N_C \leq 0.4 \cdot N_{pl,c} \\ 1.4 - \frac{N_C}{N_{pl,c}} & N_C > 0.4 \cdot N_{pl,c} \end{cases}$ | $\begin{cases} 1 & N_C \leq 0.75 \cdot N_{pl,c} \\ 1.9 - 1.2 \cdot \frac{N_C}{N_{pl,c}} & N_C > 0.75 \cdot N_{pl,c} \end{cases}$ |

# 3. Comparison with experimental data

The analytical models introduced in Section 2 have been compared against experimental results coming from the scientific literature [3,[17], [18], [19], [20], [21], [22]] in order to highlight potential inconsistencies. The selected experimental results consist of pushover tests on welded joints only, and they all exhibit a PZ failure mode. However, they differ from each other according to the type of joint being tested (exterior/interior), the presence or otherwise of transverse column web stiffeners and the presence or otherwise of an axial load in the column. Experimental results are presented in Fig. 5 in terms of moment-rotation curves, the moment $M_B$ being taken at the beam/column interface and the rotation being either the shear distortion $\gamma$ of the CWP or the total rotation $\vartheta_B$ of the joint when the former is not available (see Fig. 2).

Published in : Journal of Constructional Steel Research (2022), vol. 189, 107099
DOI: 10.1016/j.jcsr.2021.107099
Status : Postprint (Author's version)

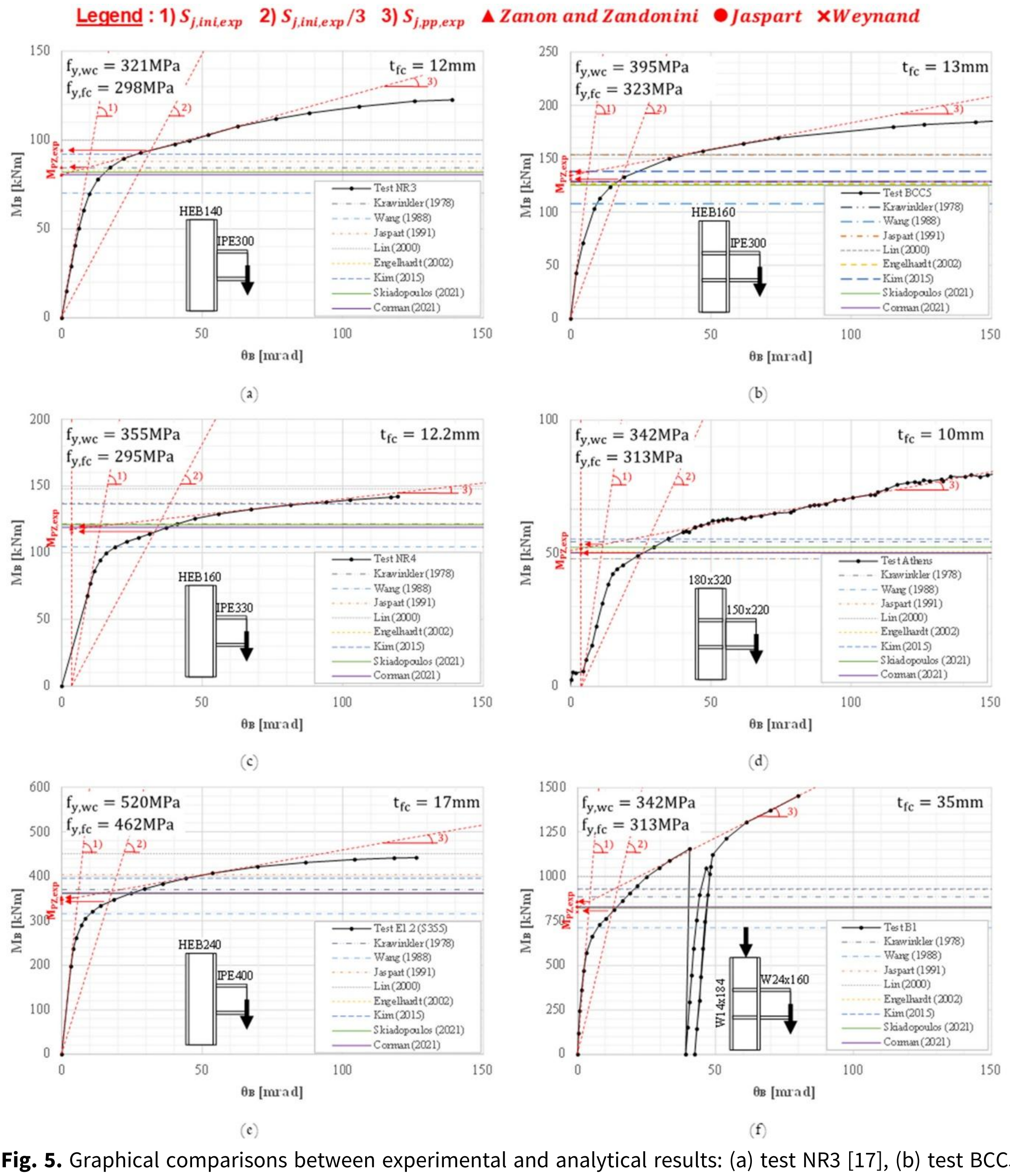


**Fig. 5.** Graphical comparisons between experimental and analytical results: (a) test NR3 [17], (b) test BCC5 [18], (c) test NR4 [17], (d) test Athens [19], (e) test E1.2 (S355) [20], (f) test B1 [3], (g) test CP-R-M [21], (h) test XU-CWP1 [22].

As a first step, it was necessary to extract the experimental plastic shear resistance of the PZ, i.e. $M_{PZ, exp}$, in order to evaluate the performance of the analytical models. The definition of $M_{PZ, exp}$ is not easy and several methods can be found in the scientific literature [23]. For instance:

- Zenon and Zandonini ([24], 1988) define $M_{PZ, exp}$ as the intersection between the initial (i.e. elastic) stiffness $S_{j, ini, exp}$ and the strain-hardening (i.e. post-plastic) stiffness $S_{j, pp, exp}$ of the curve;

- Jaspart ([9], 1991) defines $M_{PZ,exp}$ as the intersection between the y-axis and the experimental post-plastic stiffness $S_{j,pp,exp}$;
- Weynand ([25], 1997) defines $M_{PZ,exp}$ as the intersection between the experimental curve and a secant stiffness equal to one-third of the initial elastic stiffness $S_{j,ini,exp}$. This definition has been adopted by EN 1993-1-8 [15].

The authors are aware that these three definitions are highly dependent on the points chosen on the experimental curve to determine $S_{j,ini,exp}$ and $S_{j,pp,exp}$. Their accuracy is thus questionable, especially in the absence of a well-marked bi-linear behaviour of the tested joints.

Nevertheless, the three procedures were applied to the eight experimental results presented in Fig. 5 (see the graphical constructions in light red). They give very similar results in terms of $M_{PZ,exp}$ for all eight experimental results (except test NR3), which gives confidence in the so-obtained values of $M_{PZ,exp}$. These values are reported in Table 3 for the definition of Jaspart only, as this definition has been adopted by the authors for the rest of the article. Indeed, it seems to the authors that this definition is the most appropriate for evaluating the performance of rigid-plastic models such as those introduced in Section 2.

**Table 3.** Numerical comparisons between experimental and analytical results.

| Authors | NR3 | | BCC5 | | NR4 | | Athens | | E1.2 (S355) | | BI | | CP-R-M | | XU-CWPI | |
|---|---|---|---|---|---|---|---|---|---|---|---|---|---|---|---|---|
| | $M_{PZ,Rk}$ [kNm] | $E$ [%] | $M_{PZ,Rk}$ [kNm] | $E$ [%] | $M_{PZ,Rk}$ [kNm] | $E$ [%] | $M_{PZ,Rk}$ [kNm] | $E$ [%] | $M_{PZ,Rk}$ [kNm] | $E$ [%] | $M_{PZ,Rk}$ [kNm] | $E$ [%] | $M_{PZ,Rk}$ [kNm] | $E$ [%] | $M_{PZ,Rk}$ [kNm] | $E$ [%] |
| Krawinkler (1978) | 84.45 | 5.56 | 128.47 | 2.67 | 121.69 | 4.90 | 54.23 | 6.33 | 369.84 | 7.20 | 885.98 | 5.47 | 124.33 | -4.36 | 162.77 | -5.64 |
| Wang (1988) | 70.22 | -12.22 | 107.73 | -18.39 | 104.21 | -10.16 | 47.99 | -5.90 | 315.47 | -8.56 | 711.22 | -15.33 | 106.02 | -18.45 | 139.90 | -18.90 |
| Jaspart (1991) | 87.94 | 9.92 | 153.47 | 16.27 | 137.24 | 18.31 | 47.90 | -6.08 | 403.81 | 17.05 | 925.05 | 10.13 | 135.16 | 3.97 | 193.23 | 12.02 |
| Lin (2000) | 99.82 | 24.78 | 153.69 | 16.43 | 148 | 27.59 | 66.47 | 30.33 | 450.66 | 30.63 | 1000.8 | 19.14 | 155.14 | 19.34 | 200.26 | 16.09 |
| Engelhardt (2002) | 82.90 | 3.62 | 126.34 | -4.29 | 121.38 | 4.64 | 50.70 | 0.59 | 361.38 | 4.75 | 826.95 | -1.55 | 119.26 | -8.26 | 157.48 | -8.71 |
| Kim (2015) | 92.06 | 15.08 | 138.16 | 4.67 | 136.45 | 17.63 | 55.26 | 8.35 | 395.33 | 14.59 | 930.29 | 10.75 | 126.38 | -2.78 | 169.46 | -1.76 |
| Skiadopoulos (2021) | 81.92 | 2.40 | 125.31 | -5.07 | 121.2 | 4.48 | 52.24 | 2.43 | 361.76 | 4.86 | 822.70 | -2.06 | 119.95 | -7.73 | 159.15 | -7.74 |
| Corman (2021) | 80.56 | 0.70 | 128.49 | -2.66 | 118.94 | 2.53 | 50.23 | -1.51 | 362.13 | 4.97 | 829.02 | -1.31 | 128.01 | -1.53 | 175.64 | 1.82 |
| Experimental results | 80 | - | 132 | - | 116 | - | 51 | - | 345 | - | 840 | - | 130 | - | 172.5 | - |

In a second step, the plastic shear resistances were computed for each analytical model, first in terms of $V_{PZ,Rk}$ values, based on the equations introduced in Table 1, and using actual geometrical and mechanical properties of the specimens ($f_{y,wc}$ and $f_{y,fc}$ values are reported in Fig. 5 for each specimen). These $V_{PZ,Rk}$ values were then transformed into $M_{PZ,Rk}$ values by means of Eq. (1). These latter are presented in Fig. 5 and summarized in Table 3.

In Table 3, the relative errors $E$ between the experimental values $M_{PZ,exp}$ and the analytical predictions $M_{PZ,Rk}$ are also reported for each analytical model. These errors have been classified into three main categories according to the level of accuracy of the analytical model, i.e. high accuracy category if

*Published in : Journal of Constructional Steel Research (2022), vol. 189, 107099*
*DOI: 10.1016/j.jcsr.2021.107099*
*Status : Postprint (Author's version)*

$|E| \leq 5\%$ (see the light green boxes in Table 3), moderate accuracy category if $5\ \% < |E| \leq 10\%$ (see the light orange boxes in Table 3) and low accuracy category if $|E| > 10\%$ (see the light red boxes in Table 3). Based on these values, the following conclusions can be drawn regarding the performances of the different analytical models:

- The model of Krawinkler features a moderate to high level of accuracy with a relative error varying from 2.67% to 7.20%. However, this model is known to over-estimate the plastic shear resistance of the PZ in the presence of stocky columns with thick column flanges (i.e. $t_{fc} > 30 - 40mm$) [7,11,13].
- The model of Wang (resp. Lin) significantly under-estimates (resp. over-estimates) $M_{PZ,\,exp}$ in all the cases, with a relative error varying from 5.9% to 18.90% (resp. from 16.09% to 30.63%) due to the under-estimation (resp. over-estimation) of the effective shear area $A_{VC}$, as suggested in [6,11].
- The model of Jaspart features a moderate to low level of accuracy. Indeed, it tends to over-estimate (sometimes significantly) $M_{PZ,\,exp}$ in all but one cases. This observation is in line with the main conclusion drawn in [5,18], where the authors suggest the effective shear area $A_{VC}$ to be re-evaluated.
- The model of Engelhardt provides an accurate estimation of $M_{PZ,\,exp}$ (high level of accuracy) for (un-)stiffened exterior joints. However, it tends to under-estimate $M_{PZ,\,exp}$ in the case of (un-)stiffened interior joints (moderate level of accuracy). The same observations apply to the model of Skiadopoulos.
- On the other way around, the model of Kim works well (high level of accuracy) for (un-)stiffened interior joints but over-estimates (sometimes significantly) $M_{PZ,\,exp}$ in the case of (un-)stiffened exterior joints (moderate to low level of accuracy).
- The model of Corman will be described in details in Section 5. It is presented here for information purpose only.

In conclusion, none of the models introduced in Section 2 provides satisfactory results (i.e. highly accurate results) for all eight investigated cases. This shows that there is a clear need for a better understanding of the physical phenomena governing the plastic shear resistance of the PZ.

# 4. FE analysis

## 4.1. DEVELOPMENT OF A FE MODEL AND VALIDATION

In order to further investigate the conclusions drawn in Section 3, finite element (FE) analyses have been used. The role of the FE analysis is twofold: (i) developing an extensive parametric study in order to highlight the key parameters governing the plastic shear resistance of the PZ and (ii) using the so-obtained FE results in order to validate the new analytical models developed in 5 Complex

*Published in : Journal of Constructional Steel Research (2022), vol. 189, 107099*
*DOI: 10.1016/j.jcsr.2021.107099*
*Status : Postprint (Author's version)*

analytical model, 6 Towards a simplified analytical model for practice. In the present article, the commercial FE software Abaqus© [26] has been chosen to conduct the FE analyses.

As a preliminary step, the numerical tool had to be validated. To this aim, two pushover tests, namely tests NR4 and NR16, taken from [17], were numerically modelled within the Abaqus© environment. These two tests consist of an IPE330 beam welded to an HEB160 column and of an HEB500 beam welded to an HEB300 column, respectively. All actual geometrical properties may be found in [17,27] and are recalled in Table 4.

**Table 4.** Actual geometrical properties for specimens NR4 and NR16.

| Specimen | C…column B…beam | *h* [mm] | *b* [mm] | $t_w$ [mm] | $t_f$ [mm] | *r* [mm] | *A* [cm²] | *L* [mm] |
|---|---|---|---|---|---|---|---|---|
| NR4 | C…HEB160 | 159 | 160 | 8.0 | 12.2 | 15 | 51.7 | 1350 |
| | B…IPE330 | 329 | 162 | 8.0 | 11.4 | 18 | 64.2 | 698 |
| NR16 | C…HEB300 | 298 | 300 | 10.6 | 18.0 | 27 | 142.0 | 1600 |
| | B…HEB500 | 500 | 301 | 14.7 | 27.6 | 27 | 237.8 | 580 |

Fillet welds were not modelled explicitly and an initial geometrical imperfection was taken into account. The magnitude of the initial imperfection was fixed to "*d*/200", *d* being the clear depth of the column cross-section (as recommended in [28]). The Young's modulus and the Poisson's ratio were taken equal to 210,000 MPa and 0.3, respectively. Based on the available mechanical properties (i.e. the yield strength $f_y$), the complete material law was reconstructed for each specimen, using the bilinear plus non-linear hardening model proposed by Yun and Gardner for hot-rolled steels, see [29]. All mechanical properties can be found in Table 5.

**Table 5.** Mechanical properties used in the numerical simulations for specimens NR4 and NR16.

| Specimen | C…column B…beam | | $f_y$ [MPa] | $\varepsilon_{sh}$* [%] | $E_{sh}$* [MPa] | $f_u$* [MPa] | $\varepsilon_u$* [%] |
|---|---|---|---|---|---|---|---|
| NR4 | C…HEB160 | Web | 355 | 1.82 | 2279 | 485 | 16.08 |
| | | Flange | 295 | 1.73 | 1898 | 408 | 16.62 |
| | B…IPE330 | Web | 317 | 1.77 | 2037 | 436 | 16.38 |
| | | Flange | 286 | 1.74 | 1836 | 395 | 16.56 |
| NR16 | C…HEB300 | Web | 284 | 1.5 | 1972 | 440 | 21.3 |
| | | Flange | 271 | 1.5 | 1882 | 420 | 21.3 |
| | B…HEB500 | Web | 299 | 1.5 | 1988 | 440 | 19.23 |
| | | Flange | 271 | 1.5 | 1807 | 400 | 19.35 |

∗: estimated mechanical properties based on [29].

*Published in : Journal of Constructional Steel Research (2022), vol. 189, 107099*
*DOI: 10.1016/j.jcsr.2021.107099*
*Status : Postprint (Author's version)*

Both mesh density and FE type were selected based on a preliminary mesh sensitivity analysis. A coarse mesh made of eight-node brick elements with reduced integration (C3D8R) was adopted in almost all the model except for the PZ region and the column supports which were more densely meshed using fully-integrated eight-node brick elements (C3D8). The root fillets were modelled using six-node triangular prisms with full integration (C3D6). 4 finite elements were placed throughout the webs and flanges thicknesses. Fig. 6(a) gives a general overview of the final mesh used for the specimen NR4.

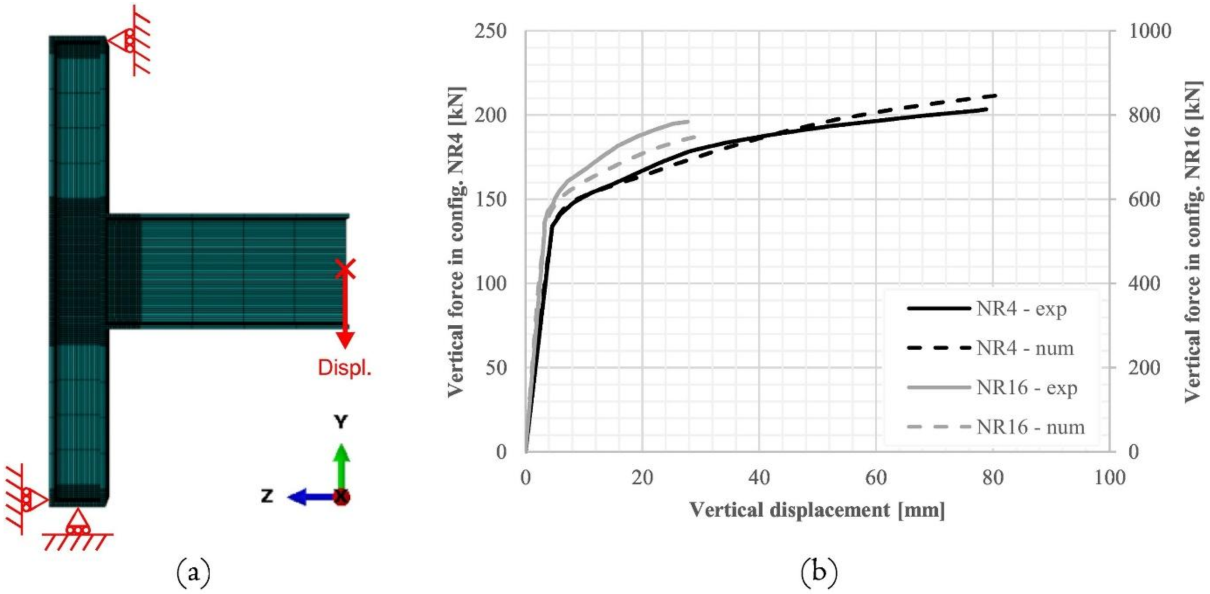


**Fig. 6.** Finite element modelling: (a) description of the mesh, (b) validation of the numerical model.

Simply-supported boundary conditions were applied to the column ends similarly to the experimental tests. A monotonic displacement history was imposed on the beam tip in order to reflect the real loading conditions. Furthermore, the beam end section was properly restrained against out-of-plane displacement. Numerical simulations were performed using a general static analysis.

The FE models were validated through comparisons between experimental (continuous lines) and numerical (dotted lines) results in terms of vertical force vs. vertical displacement at the beam tip, as shown in Fig. 6(b). Comparisons show a rather good agreement for both specimens NR4 and NR16, especially in the elasto-plastic part of the curves which is being investigated in this study. In the post-plastic part of the curves, some discrepancies can be observed. This is due to the fact that strain-hardening and ultimate properties, given in Table 5, had to be assumed, as they were not made available in [17].

## 4.2. PARAMETRIC STUDY

The so-validated numerical models were then used to perform a parametric study with the aim of appraising, one by one, the influence of 4 parameters on the plastic shear resistance of the PZ. These parameters are: (i) the spread of yielding across the PZ, (ii) the type of plastic collapse mechanism

*Published in : Journal of Constructional Steel Research (2022), vol. 189, 107099*
*DOI: 10.1016/j.jcsr.2021.107099*
*Status : Postprint (Author's version)*

which actually develops in the SE, (iii) the $\tau - \sigma_i$ interaction within the PZ and (iv) the $\tau - \sigma_{n,\ N-M}$ interaction within the PZ.

As a preliminary step to the parametric study, some slight changes were made to the original NR4 and NR16 numerical models regarding their geometrical and material properties. These changes aim at making the parametric study as general as possible and they are listed here below:

- the column supports were moved towards the column centreline;
- the column length $L_c$ was increased to 4 m in order to reduce the influence of the support reactions;
- the beam length $L_b$ was increased in such a way that the distance between the column centreline and the beam end is 1.5 m;
- actual geometrical properties of the steel profiles were replaced by nominal ones;
- actual material laws were replaced by an elastic-perfectly plastic one (i.e. strain-hardening neglected) for all members to facilitate the derivation of the plastic shear resistance of the PZ;
- S355 steel grade with nominal yield strength was considered for all members.

In order to broaden the parametric study, two additional models, named A and B, were added to the study. These models are characterized by an IPE200 beam welded to an HEB160 column and by an IPE300 beam welded to an HEB340 column, respectively. A summary of the four beam-to-column assemblies considered in the present study is given in Table 6. These numerical models were then used to perform the parametric study, which covers the following 8 joint configurations:

- (non-)axially loaded (un-)stiffened exterior joints;
- (non-)axially loaded (un-)stiffened interior joints.

**Table 6.** Details of the configurations studied in the parametric study

| **Model** | **Column profile** | **Beam profile** | **Stiffener thickness $t_{st}$ [mm]** | **Axial load $N$ [kN]** | **Column web-to-flange thickness ratio $t_{wc}/t_{fc}$ [−]** |
|---|---|---|---|---|---|
| NR4 | HEB160 | IPE330 | 12 | 1000 | 0.615 |
| NR16 | HEB300 | HEB500 | 30 | 2500 | 0.579 |
| A | HEB160 | IPE200 | 10 | 1000 | 0.615 |
| B | HEB340 | IPE300 | 12 | 3000 | 0.558 |

The thickness $t_{st}$ of the transverse column web stiffeners, if any, is given in Table 6. The magnitude of the axial load $N$ in the column, if any, was set at $0.5N_{pl}$, $N_{pl}$ being the axial strength of the column cross-section. This load level is assumed to be representative of the maximum axial load which may be encountered by a column in a typical steel frame structure. These values are summarized in Table 6 too. Finally, Table 6 also shows the column web-to-flange thickness ratios. This parameter

*Published in : Journal of Constructional Steel Research (2022), vol. 189, 107099*
*DOI: 10.1016/j.jcsr.2021.107099*
*Status : Postprint (Author's version)*

oscillates between 0.55 and 0.62 which is the range of validity for all the developments presented in this article.

A specific nomenclature has been adopted in order to identify the different simulations: for instance, the numerical simulation performed on the unstiffened (i.e. "0") exterior (i.e. single-sided, "s") NR4 joint configuration without any axial load in the column (i.e. "/") is named "NR4–0-s–/". By contrast, the numerical simulation performed on the stiffened (i.e. "1") interior (i.e. double-sided, "d") NR16 joint configuration with an axial load in the column (i.e. "$0.5N_{pl}$") is named "NR16–1-d-$0.5N_{pl}$".

In total, 32 numerical simulations were performed in the framework of the parametric study. The component method was applied to each of them, in accordance with EN 1993-1-8 [15], and showed that all the joint configurations are characterized by a PZ failure mode, except the exterior joints in the B series which are characterized by a "beam flange in compression" (BFC) failure mode. Therefore, the numerical results of these latter are not accounted for in the following sections.

## 4.3. FE RESULTS AND DISCUSSION

The results from the parametric study are presented in Fig. 7 in terms of equivalent shear force ($V_{PZ}$) vs. shear distortion ($\gamma$) curves, $V_{PZ}$ being given by Eq. (1), and $\gamma$ being defined in Fig. 2. In addition, 12 $\sigma_{VM}$, $\tau$, $\sigma_{n,\,N-M}$ and $\sigma_i$ states of stress, coming from Abaqus©, are given in Table 7 and Table 8. These states of stress have been identified based on the careful analysis of the FE results and they were considered relevant for the illustration of the different conclusions given in 4.3.1 Study of the spread of yielding across the PZ, 4.3.2 Study of the collapse mechanism which actually develops in the SE, 4.3.3 Influence of the τ − σ, 4.3.5 Conclusion of the parametric study. They belong to the configurations NR4–1-d–/, NR4–0-s–/, NR4–1-d-0.5Npl and NR4–0-s-0.5Npl respectively, i.e. 3 states of stress per configuration; these ones are identified in Fig. 7 (dots 1 to 12).

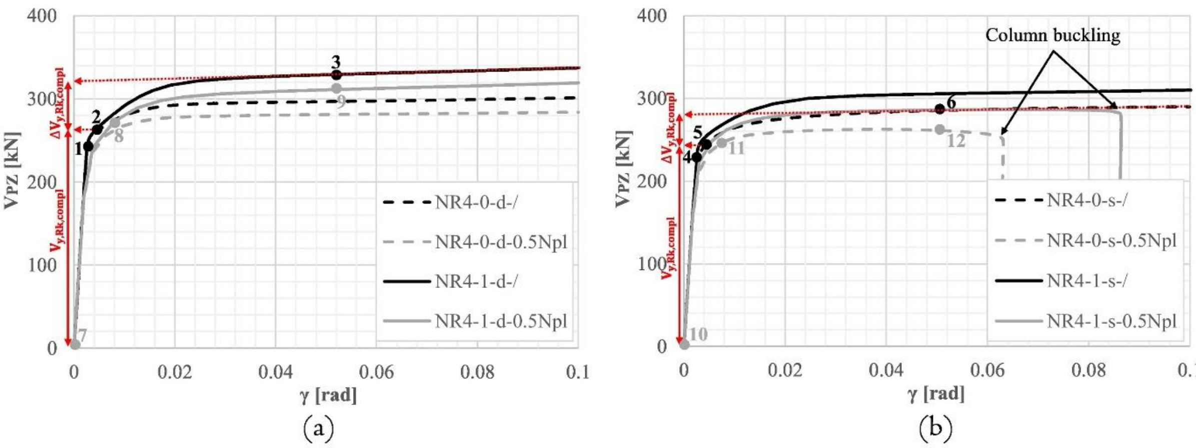


**Fig. 7.** Numerical results for the model NR4 (in terms of $V_{PZ} - \gamma$ curves): (a) interior joints, (b) exterior joints.

*Published in : Journal of Constructional Steel Research (2022), vol. 189, 107099*
*DOI: 10.1016/j.jcsr.2021.107099*
*Status : Postprint (Author's version)*

**Table 7.** Description of the 6 relevant states of stress introduced in Fig. 7(a) and Fig. 7(b) for the configurations NR4–1-d−/ and NR4–0-s−/ (in terms of $\sigma_{VM}$, $\tau$, $\sigma_{n,N-M}$ and $\sigma_i$ stresses).

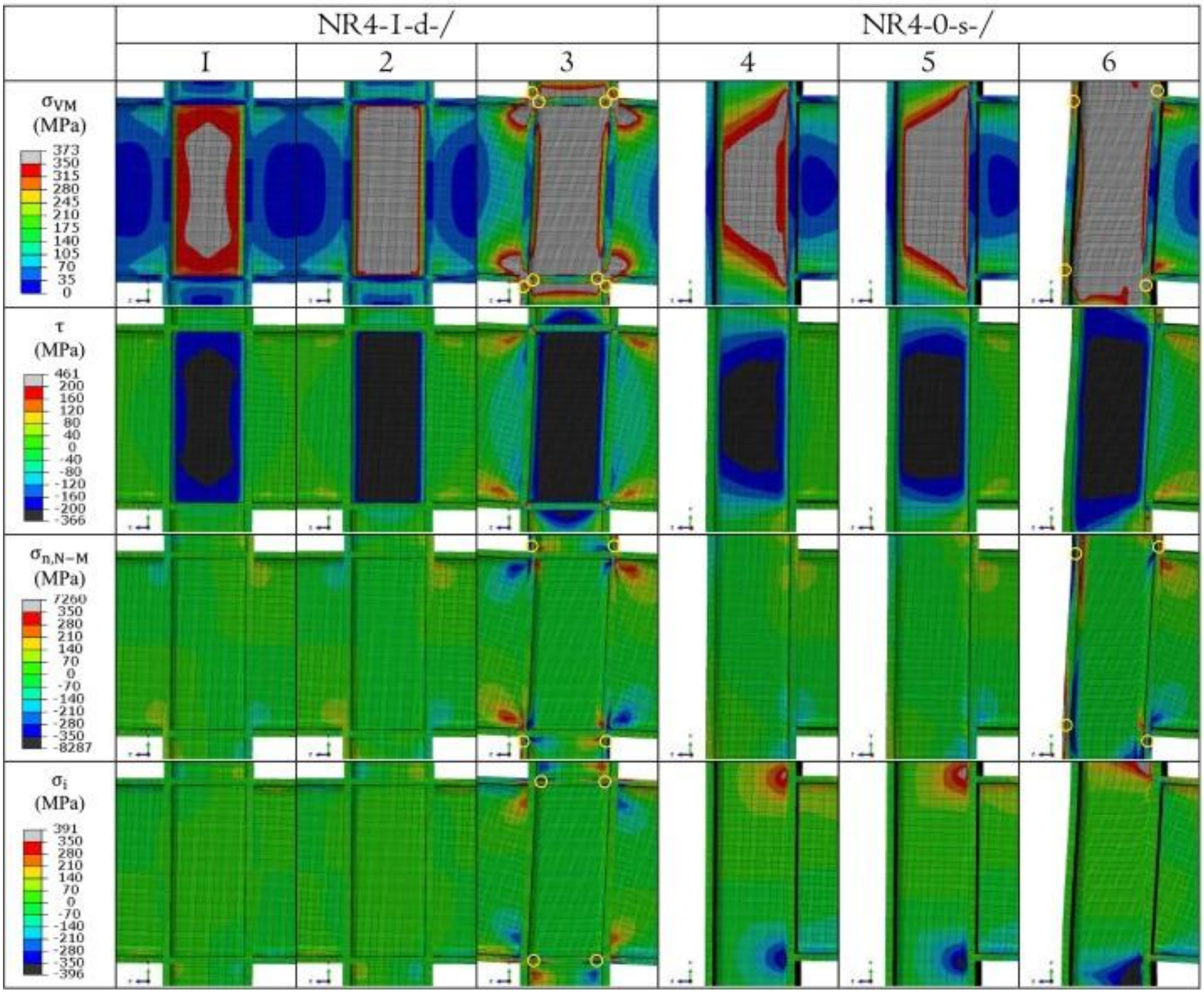

Published in : Journal of Constructional Steel Research (2022), vol. 189, 107099
DOI: 10.1016/j.jcsr.2021.107099
Status : Postprint (Author's version)

**Table 8.** Description of the 6 relevant states of stress introduced in Fig. 7(a) and Fig. 7(b) for the configurations NR4–1-d-0.5Npl and NR4–0-s-0.5Npl (in terms of $\sigma_{VM}$, $\tau$, $\sigma_{n,N-M}$ and $\sigma_i$ stresses).

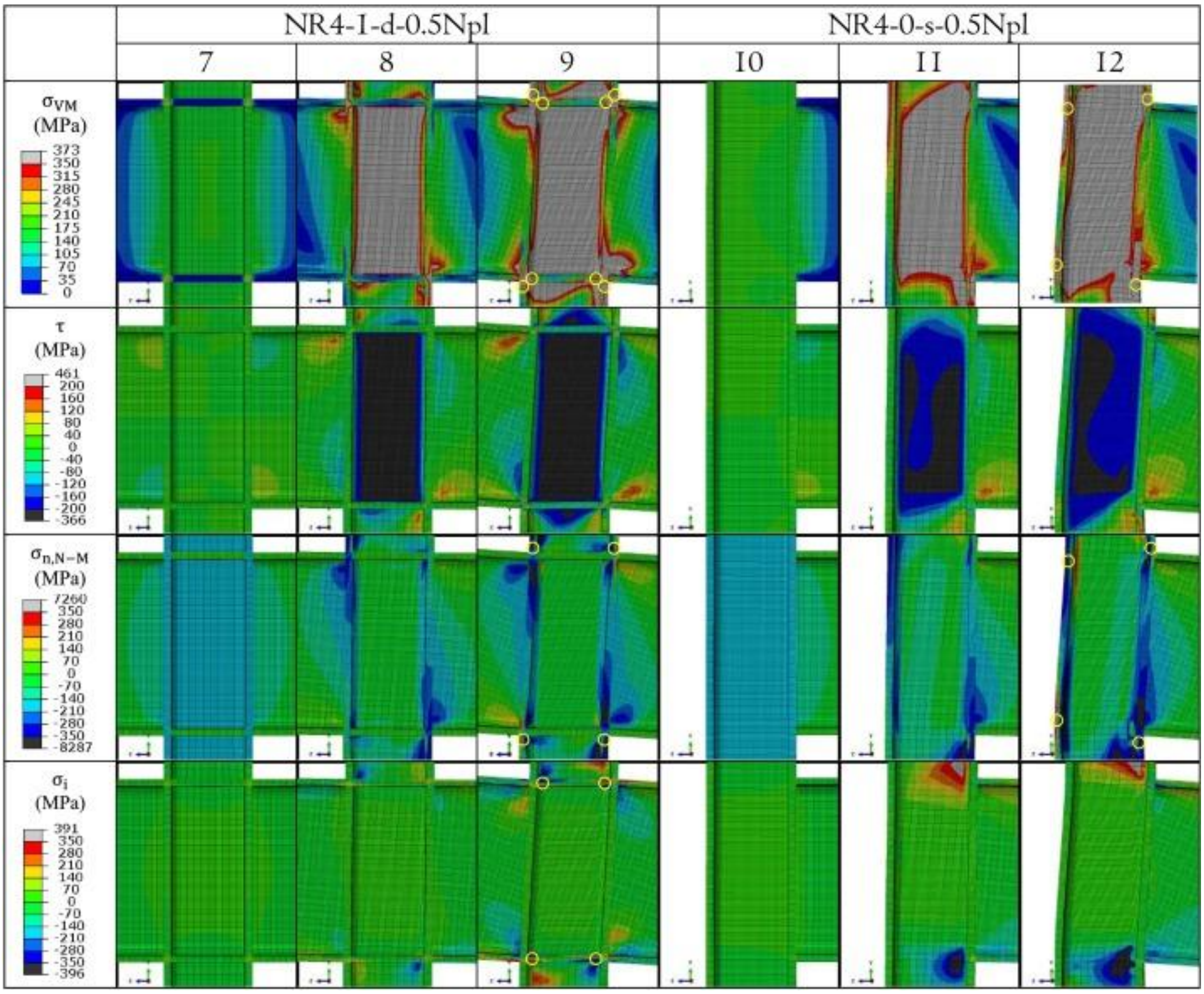


Results are presented here for the model NR4 only but similar results were obtained for the models NR16, A and B. Therefore, the conclusions drawn from Fig. 7, Table 7 and Table 8 and presented here below are also valid for the models NR16, A and B. In total, four main observations were made from the parametric study, regarding: (i) the spread of yielding across the PZ, (ii) the type of plastic collapse mechanism which actually develops in the SE, (iii) the influence of the $\tau - \sigma_i$ interaction on the plastic shear resistance of the PZ and (iv) the influence of the $\tau - \sigma_{n,N-M}$ interaction on the plastic shear resistance of the PZ. These observations are described in details in the following 4.3.1 Study of the spread of yielding across the PZ, 4.3.2 Study of the collapse mechanism which actually develops in the SE, 4.3.3 Influence of the $\tau - \sigma$, 4.3.5 Conclusion of the parametric study and will serve as the basis for the development of the new complex analytical model in Section 5.

### 4.3.1. STUDY OF THE SPREAD OF YIELDING ACROSS THE PZ

Regarding the spread of yielding across the PZ, the following observations were made [5]:

- Yielding initiates in the centre of the CWP and is not affected by the SE, as depicted by the states of stress No. 1 and No. 4 in Table 7, the black parts on the pictures being the parts yielding in pure shear. This is due to the fact that the shear stiffness of the CWP is significantly larger than that of the SE, and so the CWP first "attracts" most of the forces.

- Yielding very quickly spreads across the entire panel, as depicted by the states of stress No. 2 and No. 5 in Table 7, the plastic shear resistance of the CWP being reached for a $V_{y,\,Rk,\,compl}$ value. This contribution is highlighted in red in Fig. 7(a) and Fig. 7(b) for two particular configurations (i.e. configurations NR4–1-d−/ and NR4–0-s−/). For this shear level, it can be seen that solely the clear depth of the CWP strictly speaking yields. Therefore, it is suggested to account for the actual shear stress distribution in the derivation of $V_{y,\,Rk,\,compl}$.
- Extra shear forces are then transferred to the SE, which contribute to the resistance of the PZ with a $\Delta V_{y,\,Rk,\,compl}$ value before large plastic rotations develop (see the states of stress No.3 and No.6 in Table 7). This second contribution is highlighted in red in Fig. 7(a) and Fig. 7(b) for two particular configurations (i.e. configurations NR4–1-d−/ and NR4–0-s−/).

#### 4.3.2. STUDY OF THE COLLAPSE MECHANISM WHICH ACTUALLY DEVELOPS IN THE SE

Regarding the collapse mechanism which develops in the SE, the following observations were made:

- In the absence of transverse column web stiffeners, four plastic hinges form in the column flanges at the level of the beam flanges (see the states of stress No. 6 and 12 in Table 7 and Table 8).
- In the presence of transverse column web stiffeners, additional plastic hinges form either in the beam(s) flanges or in the transverse column web stiffeners (see the states of stress No. 3 and No. 9 in Table 7 and Table 8). These additional plastic hinges have to be explicitly accounted for in the derivation of the contribution $\Delta V_{y,\,Rk,\,compl}$. A similar observation was made by other researchers [30,31].
- N.B.: The difference in the number of required additional plastic hinges is a first reason for the difference in strength observed between the interior and exterior joints in Fig. 7(a) and (b). Another reason comes from the influence of the $\tau - \sigma_i$ interaction and is discussed hereafter in Section 4.3.3.

#### 4.3.3. INFLUENCE OF THE Τ – ΣI INTERACTION

Regarding the influence of the $\tau - \sigma_i$ interaction, the following observations were made:

- This interaction has been neglected by all the authors in the models introduced in Section 2, the load-introduction phenomenon being assumed to be a localized phenomenon and hence not affecting the plastic shear resistance of the PZ.
- For interior joints, this assumption seems reasonable as half of the "load-introduction" force is introduced on each side of the column profile. Consequently, no significant $\sigma_i$ stress is observed within the CWP (see the $\sigma_i$ stresses in the states of stress No. 1–3 and No. 7–9 in Table 7 and Table 8).

*Published in : Journal of Constructional Steel Research (2022), vol. 189, 107099*
*DOI: 10.1016/j.jcsr.2021.107099*
*Status : Postprint (Author's version)*

- For exterior joints, this assumption is much more questionable, as it is shown in Table 7 and Table 8 (see the $\sigma_i$ stresses in the states of stress No. 4–6 and No. 10–12) that significant $\sigma_i$ stresses develop in the CWP at the level of the beam flanges, where loads are introduced in the PZ. This leads to an overall decrease in the level of shear strength for the exterior joints, with respect to the interior joints. This observation can be contemplated in Fig. 7, where the $V_{PZ} - \gamma$ curves of the exterior joints (see Fig. 7(b)) are lower than those of the corresponding interior joints (see Fig. 7(a)).
- Therefore, it is suggested to explicitly account for the $\tau - \sigma_i$ interaction in the assessment of the contribution $V_{y, Rk, compl}$ of the CWP, for the exterior joints only.

### 4.3.4. INFLUENCE OF THE $\boldsymbol{T} - \boldsymbol{\Sigma}_{N, N\text{–}M}$ INTERACTION

Finally, regarding the influence of the $\tau - \sigma_{n, N\text{–}M}$ interaction, the following observations were made:

- The comparisons between the black and grey curves in Fig. 7(a) and Fig. 7(b) show that the axial force applied to the column reduces the resistance of the PZ. Therefore, its effect has to be taken into account in both $V_{y, Rk, compl}$ and $\Delta V_{y, Rk, compl}$ contributions.
- $\sigma_{n,\ N\text{–}M}$ stresses feature a uniform distribution across the column cross-section at the beginning of the simulation, before shear is introduced into the PZ and therefore in the absence of any moment $M_C$ in the column. This observation is shown in Table 8 (see the $\sigma_{n, N\text{–}M}$ stresses in the states of stress No. 7 and No. 10).
- Once shear is introduced into the PZ, redistribution of forces occurs. The CWP, whose shear stiffness is significantly larger than that of the SE, "attracts" most of the shear force. By contrast, the SE, whose axial stiffness is significantly larger than that of the CWP, "attracts" most of the axial force. This observation is shown in Table 8 (see the $\sigma_{n, N\text{–}M}$ stresses in the states of stress No. 8, No. 9, No. 11 and No. 12). A similar observation was made by other researchers [7,9,12,32].

### 4.3.5. CONCLUSION OF THE PARAMETRIC STUDY

In conclusion, the parametric study clearly indicates that the behaviour of the PZ can always be divided into the contributions of the CWP ($V_{y, Rk, compl}$) and the SE ($\Delta V_{y, Rk, compl}$), as follows:

$$V_{PZ,Rk,compl} = V_{y,Rk,compl} + \Delta V_{y,Rk,compl} \quad (6)$$

This formalism is similar to Eq. (2). However, both contributions need to be re-evaluated. The contribution $V_{y,\ Rk,\ compl}$ of the CWP has to more accurately account for the actual shear stress distribution at yielding, as well as for both $\tau - \sigma_i$ and $\tau - \sigma_{n,\ N\text{–}M}$ interactions. It is re-evaluated in Section 5.1. The contribution $\Delta V_{y, Rk, compl}$ of the SE has to reflect more accurately the plastic collapse mechanism which actually develops and has to account for the influence of the axial load in the column flanges. It is re-evaluated in Section 5.2.

*Published in : Journal of Constructional Steel Research (2022), vol. 189, 107099*
*DOI: 10.1016/j.jcsr.2021.107099*
*Status : Postprint (Author's version)*

# 5. Complex analytical model

## 5.1. CONTRIBUTION $V_{Y, RK, COMPL}$ OF THE CWP

Based on the conclusions drawn from the parametric study, it has been decided to express the contribution $V_{y, Rk, compl}$ of the CWP through Eq. (7), as the product of the plastic shear resistance of the CWP with no stress interaction ($V^{*}_{y, Rk, compl}$), multiplied by two reduction factors, i.e. $\chi_i$ and $\chi_{n, N-M}$, accounting for the $\tau - \sigma_i$ and $\tau - \sigma_{n, N-M}$ interactions, respectively. The $\tau - \sigma_i - \sigma_{n, N-M}$ interaction, if any, is included in the two aforementioned coefficients.

$$V_{y,Rk,compl} = \chi_{n,N-M} \cdot \chi_i \cdot V^{*}_{y,Rk,compl} \quad (7)$$

Each of the 3 parameters involved in Eq. (7) was assessed based on the results of the FE simulations. To this aim, a numerical estimation ($V_{y, Rk, num}$) of the plastic shear resistance of the CWP had to be derived for each of the 28 numerical simulations. This was done following a 4-step numerical integration procedure, as described here below:

- The first step consists in isolating the PZ from the numerical model, as depicted in Fig. 8(a) and (b). The PZ is assumed to be constituted of $n$ rows of FE over its depth $d_b$.

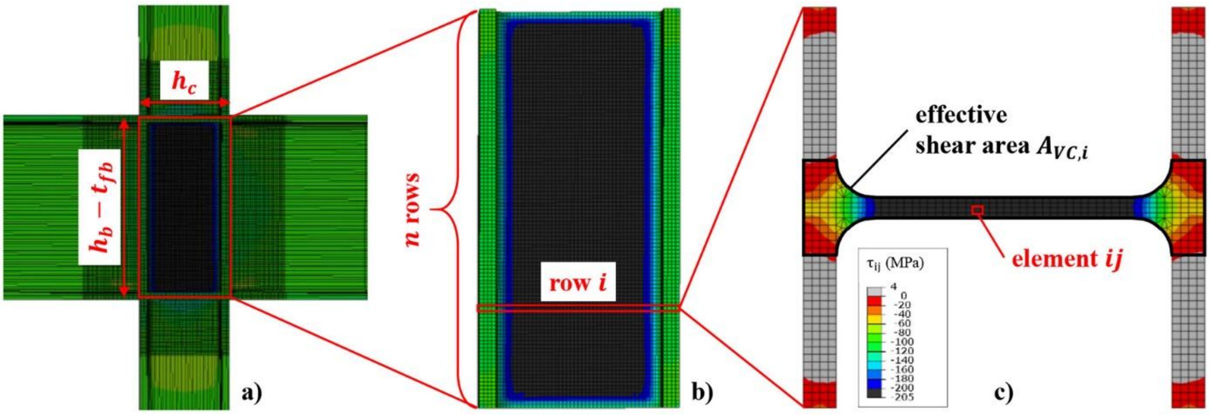


**Fig. 8.** Procedure of numerical integration: (a) numerical model (NR4–1-d−/), (b) isolation of the PZ, (c) isolation of the i[th] row of FE.

- The second step consists in isolating the $i^{th}$ row of FE, as depicted in Fig. 8(b) and (c). For this $i^{th}$ row of FE, shear stresses were integrated over the numerical effective shear area $A^{t}_{VC, i}$, highlighted in black in Fig. 8(c), thus providing one numerical value $V^{t}_{y, Rk, row, i}$. This value characterizes the shear resistance of the $i^{th}$ row of FE at time step $t$, as expressed through Eq. (8). Given the discrete FE mesh, the surface integral in Eq. (8) has been replaced by the summation of the shear level of each of the $N$ elements placed over $A^{t}_{VC, i}$, where the parameters $a^{t}_{ij}$ and $\tau^{t}_{ij}$ in Eq. (8) represent the shear stress and the area of the $j^{th}$ element in the $i^{th}$ row of FE at time step $t$, respectively.
- Eq. (9) was then applied to each of the $n$ rows of FE constituting the PZ. The average of these $n$ values is assumed to provide a rather reliable numerical estimation $V^{t}_{y, Rk, num}$ of the plastic shear resistance of the CWP at time step $t$, as expressed through Eq. (9).

*Published in : Journal of Constructional Steel Research (2022), vol. 189, 107099*
*DOI: 10.1016/j.jcsr.2021.107099*
*Status : Postprint (Author's version)*

- The numerical estimation $V_{y,\,Rk,\,num}$ of the plastic shear resistance of the CWP is eventually derived as the maximum of the numerical estimation $V^{t}_{y,\,Rk,\,num}$ obtained at each time step $t$, as expressed through Eq. (10).

$$V^t_{y,Rk,row,i} = \int_{A^t_{VC,i}} \tau d\, A^t_{VC,i} = \sum_{j=1}^{N} a^t_{ij} \cdot \tau^t_{ij} \quad (8)$$

$$V^t_{y,Rk,num} = \frac{1}{n} \sum_{i=1}^{n} \sum_{j=1}^{N} a^t_{ij} \cdot \tau^t_{ij} \quad (9)$$

$$V_{y,Rk,num} = \max_t\left(V^t_{y,Rk,num}\right) \quad (10)$$

Results are summarized in Table 9. They have been sorted into four categories, so as to facilitate the derivation of the 3 parameters involved in Eq. (7):

- Category I includes the results of the numerical simulations performed on the non-axially loaded (un-)stiffened interior joints (i.e. 8 in total, see Table 9). In these simulations, both $\tau - \sigma_i$ and $\tau - \sigma_{n,\,N\text{–}M}$ interactions are small enough to be neglected, i.e. $\chi_i$ and $\chi_{n,\,N\text{–}M}$ can be assumed equal to 1.0 in Eq. (7). ⇒ These results were used to assess the parameter $V_{y,\,Rk,\,compl}{}^*$ in Eq. (7).
- Category II includes the results of the numerical simulations performed on the non-axially loaded (un-)stiffened exterior joints (i.e. 6 in total, see Table 9). In these simulations, the $\tau - \sigma_i$ interaction is maximum while the $\tau - \sigma_{n,\,N\text{–}M}$ interaction can be neglected, i.e. $\chi_{n,\,N\text{–}M}$ is equal to 1.0 in Eq. (7). ⇒ These results were used to assess the parameter $\chi_i$ in Eq. (7).
- Category III includes the results of the numerical simulations performed on the axially loaded (un-)stiffened interior joints (i.e. 8 in total, see Table 9). In these simulations, the $\tau - \sigma_{n,\,N\text{–}M}$ interaction is maximum while the $\tau - \sigma_i$ interaction can be neglected, i.e. $\chi_i$ is equal to 1.0 in Eq. (7). ⇒ These results were used to assess the parameter $\chi_{n,\,N\text{–}M}$ in Eq. (7).
- Category IV includes the results of the numerical simulations performed on the axially loaded (un-)stiffened exterior joints (i.e. 6 in total, see Table 9). In these simulations, both $\tau - \sigma_i$ and $\tau - \sigma_{n,\,N\text{–}M}$ interactions are maximum. ⇒ These results were used to assess the parameters $\chi_i$ and $\chi_{n,\,N\text{–}M}$ in Eq. (7).

**Table 9.** Results $V_{y,\,Rk,\,num}$ of the numerical integration for each joint configuration (in [kN]).

| **Configuration** | **Category I** | **Category II** | **Category III** | **Category IV** |
|---|---|---|---|---|
| | **X="d", Y="/"** | **X="s", Y="/"** | **X="d", Y="0.5N$_{pl}$"** | **X="s", Y="0.5N$_{pl}$"** |
| NR4-0-X-Y | 256.3 | 251.9 | 244.1 | 233.4 |
| NR4-1-X-Y | 258.8 | 253.7 | 245.9 | 239.4 |
| NR16-0-X-Y | 684.4 | 657.1 | 657.5 | 619.6 |
| NR16-1-X-Y | 701.9 | 668.6 | 672.6 | 638.1 |
| A-0-X-Y | 268.5 | 255.2 | 252.8 | 238.0 |
| A-1-X-Y | 270.1 | 261.1 | 254.4 | 245.7 |
| B-0-X-Y | 851.2 | - | 804.0 | - |
| B-1-X-Y | 851.6 | - | 811.6 | - |

*Published in : Journal of Constructional Steel Research (2022), vol. 189, 107099*
*DOI: 10.1016/j.jcsr.2021.107099*
*Status : Postprint (Author's version)*

### 5.1.1. ESTIMATION OF $V^*_{Y,\,RK,\,COMPL}$

In order to assess the plastic shear resistance $V^*_{y,\,Rk,\,compl}$ of the CWP with no stress interaction, reference was made to the FE results of the category I only, for which $\chi_i$ and $\chi_{n,\,N\text{–}M}$ are both equal to 1.0 (i.e. $V_{y,\,Rk,\,num} = V^*_{y,\,Rk,\,num}$), and to the procedure reported in [5]. The main steps are recalled here below:

- For these simulations, it is observed a uniform distribution of the shear stress $\tau$ at yielding over the whole depth $d_b$of the PZ, as depicted in Fig. 8(a) and (b). Therefore, the $i^{th}$ row of FE can be arbitrarily extracted from the PZ, as depicted in Fig. 8(c). For sake of clarity, this $i^{th}$ row of FE has been duplicated in Fig. 9(a) where the shear stress distribution over $A_{VC}$ has been studied.

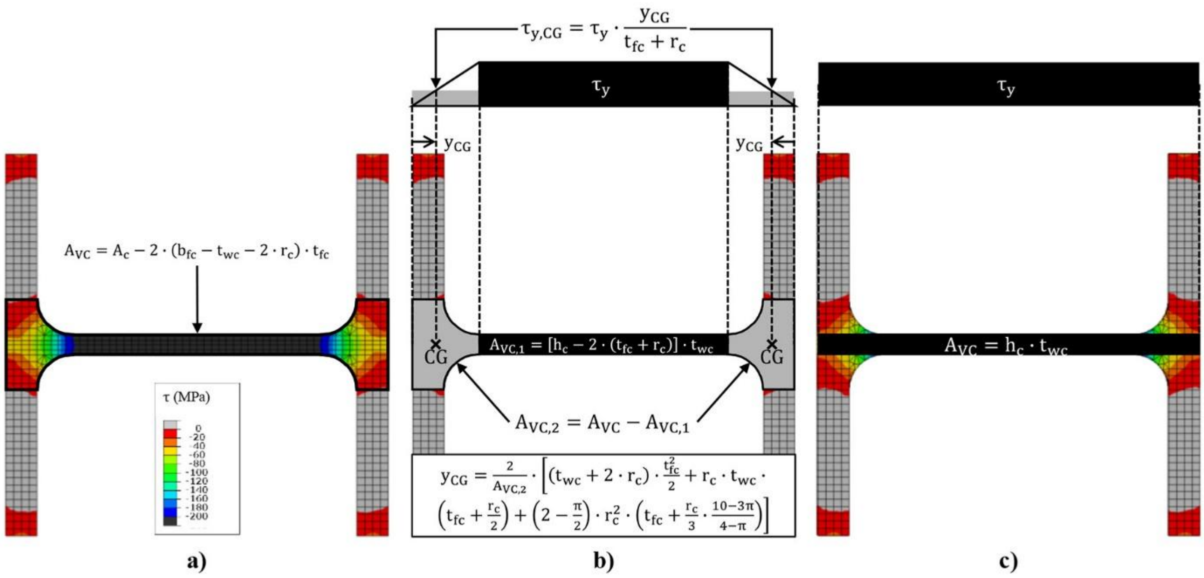


**Fig. 9.** Shear stress distribution at yielding: (a) FE results, (b) complex analytical model, (c) simplified analytical model.

- From Fig. 9(a), it can be seen that, strictly speaking, solely the clear depth of the column cross-section yields. Therefore, a uniform shear stress distribution was considered over the area $A_{VC1}$, as depicted by the black rectangles in Fig. 9(b).

- It was secondly observed that, when the flow of shear stress reaches the root fillets and the flanges of the column cross-section, it spreads over a larger area $A_{VC2}$, which coincides with a general decrease in the shear stress level. Therefore, a linearly decreasing shear stress distribution can be assumed over $A_{VC2}$, varying from $\tau_y$ at the onset of the root fillets to 0 at the extremity of the column flanges, as shown in Fig. 9(b).

- The integration of the triangular shear stress profile over $A_{VC2}$ is not easy. Therefore, a simplified procedure is proposed, which consists in: (i) computing the location $y_{CG}$ of the centre of gravity of $A_{VC2}$ (see the formula in Fig. 9(b)), (ii) deriving the shear stress level $\tau_{y,\,CG}$ at the centre of gravity of $A_{VC2}$ (based on the aforementioned assumption of a triangular shear stress distribution over $A_{VC2}$, see Fig. 9(b)), (iii) using $\tau_{y,\,CG}$ as the mean shear stress over the whole area $A_{VC2}$ as depicted by the grey rectangles in Fig. 9(b).

*Published in : Journal of Constructional Steel Research (2022), vol. 189, 107099*
*DOI: 10.1016/j.jcsr.2021.107099*
*Status : Postprint (Author's version)*

- Therefore, the analytical estimation of the plastic shear resistance $V^{*}_{y,Rk,compl}$ of the CWP with no stress interaction may be expressed through Eq. (11) as the sum of the black and grey contributions presented in Fig. 9(b).

Analytical and numerical results for the joints of category I are compared in Table 10 and show a good agreement, provided that a 0.95 reduction coefficient is affected to Eq. (11). This way, the ratio between the two oscillates a bit below 1.0, while the maximum relative error remains lower than 3%. Simplifications of this rather complex approach will be discussed later in Section 6.

**Table 10.** Comparison between $V^{*}_{y,Rk,compl}$ and $V^{*}_{y,Rk,num}$.

| Configuration | Interior joints $V^{*}_{y,Rk,compl}$ [kN] | Interior joints $V^{*}_{y,Rk,num}$ [kN] | Ratio $\frac{V^{*}_{y,Rk,compl}}{V^{*}_{y,Rk,num}}$ [-] |
|---|---|---|---|
| NR4-0-d-/ | 262.8 | 256.3 | 1.025 |
| NR4-1-d-/ | 262.8 | 258.8 | 1.015 |
| NR16-0-d-/ | 692.8 | 684.4 | 1.012 |
| NR16-1-d-/ | 692.8 | 701.9 | 0.987 |
| A-0-d-/ | 262.8 | 268.5 | 0.979 |
| A-1-d-/ | 262.8 | 270.1 | 0.973 |
| B-0-d-/ | 850.5 | 851.2 | 0.999 |
| B-1-d-/ | 850.5 | 851.6 | 0.999 |
| | | Mean value | 0.999 |

NB: It is likely that the shear stress distribution is influenced by the column web-to-flange thickness ratio $t_{wc}/t_{fc}$. The 0.95 reduction coefficient adopted in Eq. (11) is valid for the range of column web-to-flange thickness ratios considered in this article (i.e. 0.55 – 0.62, see Table 6). This range includes 40% of the European HE-profiles (total range: $0.515 \leq t_{wc}/t_{fc} \leq 0.78$) and 55% of the American W-profiles (total range: $0.525 \leq t_{wc}/t_{fc} \leq 0.905$). However, additional simulations would be required in order to validate this 0.95 reduction coefficient to the whole range of European HE-profiles and American W-profiles.

$$V^{*}_{y,Rk,compl} = 0.95 \cdot \left(A_{VC,1} \cdot \tau_y + 2 \cdot A_{VC,2} \cdot \tau_{y,CG}\right) \quad (11)$$

### 5.1.2. ESTIMATION OF $X_I$

In order to assess the reduction factor $\chi_i$ accounting for the $\tau - \sigma_i$ interaction, the FE results coming from the categories II and IV (i.e. exterior joints where the $\tau - \sigma_i$ interaction is maximum) were compared to their corresponding FE results coming from the categories I and III (i.e. interior joints where the $\tau - \sigma_i$ interaction is minimum). This is done in Table 11. As the ratio between the two oscillates a bit above 0.95, the value of $\chi_i$ has been set at 0.95 for exterior joints while it remains equal to 1.0 in the case of interior joints, as summarized in Table 13.

*Published in : Journal of Constructional Steel Research (2022), vol. 189, 107099*
*DOI: 10.1016/j.jcsr.2021.107099*
*Status : Postprint (Author's version)*

**Table 11.** Determination of the reduction factor $\chi_i$.

| Configuration | Exterior joints (X="s") $V_{y,Rk,num}(s)$ [kN] | Interior joints (X="d") $V_{y,Rk,num}(d)$ [kN] | Ratio $\chi_i$ $\frac{V_{y,Rk,num}(s)}{V_{y,Rk,num}(d)}$ [-] |
|---|---|---|---|
| NR4-0-X-/ | 251.9 | 256.3 | 0.983 |
| NR4-I-X-/ | 253.7 | 258.8 | 0.980 |
| NR16-0-X-/ | 657.1 | 684.4 | 0.960 |
| NR16-I-X-/ | 668.6 | 701.9 | 0.953 |
| A-0-X-/ | 255.2 | 268.5 | 0.950 |
| A-I-X-/ | 261.1 | 270.1 | 0.967 |
| NR4-0-X-0.5$N_{pl}$ | 233.4 | 244.1 | 0.956 |
| NR4-I-X-0.5$N_{pl}$ | 239.4 | 245.9 | 0.974 |
| NR16-0-X-0.5$N_{pl}$ | 619.6 | 657.5 | 0.942 |
| NR16-I-X-0.5$N_{pl}$ | 638.1 | 672.6 | 0.949 |
| A-0-X-0.5$N_{pl}$ | 238.0 | 252.8 | 0.941 |
| A-I-X-0.5$N_{pl}$ | 245.7 | 254.4 | 0.966 |
| | | Mean value | 0.96 |

N.B.: This value may be a bit conservative in the case of stiffened exterior joints as the stiffeners are known to attract part of the "load-introduction" forces, thus reducing the $\tau - \sigma_i$ interaction in the CWP. However, given the low influence of this parameter on the plastic shear resistance of the PZ, $\chi_i$ has been kept equal to 0.95 for both (un-)stiffened exterior joints, for sake of simplicity of the analytical model.

### 5.1.3. ESTIMATION OF $\chi_{N,\,N-M}$

Similarly to $\chi_i$, the reduction factor $\chi_{n,\,N-M}$ was assessed through comparisons between the FE results coming from categories III and IV (i.e. axially loaded joints where the $\tau - \sigma_{n,\,N-M}$ interaction is maximum) and their corresponding FE results coming from the categories I and II (i.e. non-axially loaded joints where the $\tau - \sigma_{n,\,N-M}$ interaction is minimum). These comparisons are given in Table 12 and show that the ratio between the two oscillates around 0.95. Thus, the axial load has little influence on the plastic shear resistance $V_{y,\,Rk,\,compl}$ of the CWP. As a consequence and for sake of simplicity of the analytical model, the value of $\chi_{n,\,N-M}$ has been set at 0.95 for all axially loaded joints (i.e. $N \leq 0.5N_{pl}$) while it remains equal to 1.0 in the absence of any axial load in the column, as summarized in Table 13. This reduction factor $\chi_{n,\,N-M}$ needs however to be re-evaluated for higher axial loads (i.e. $N > 0.5N_{pl}$) as well as for column profiles characterized by different web-to-flange thickness ratios than those considered in the present article, especially those with thin flanges and thick webs.

*Published in : Journal of Constructional Steel Research (2022), vol. 189, 107099*
*DOI: 10.1016/j.jcsr.2021.107099*
*Status : Postprint (Author's version)*

**Table 12.** Determination of the reduction factor $\chi_{n,\,N-M}$.

| Configuration | Axial load (Y="0.5N$_{pl}$") $V_{y,Rk,num}(0.5N_{pl})$ [kN] | No axial load (Y="/") $V_{y,Rk,num}(/)$ [kN] | Ratio $\chi_{n,N-M}$ $\frac{V_{y,Rk,num}(0.5N_{pl})}{V_{y,Rk,num}(/)}$ [-] |
|---|---|---|---|
| NR4-0-d-Y | 244.1 | 256.3 | 0.952 |
| NR4-1-d-Y | 245.9 | 258.8 | 0.950 |
| NR4-0-s-Y | 233.4 | 251.9 | 0.961 |
| NR4-1-s-Y | 239.4 | 253.7 | 0.944 |
| NR16-0-d-Y | 657.5 | 684.4 | 0.961 |
| NR16-1-d-Y | 672.6 | 701.9 | 0.958 |
| NR16-0-s-Y | 619.6 | 657.1 | 0.943 |
| NR16-1-s-Y | 638.1 | 668.6 | 0.954 |
| A-0-d-Y | 252.8 | 268.5 | 0.942 |
| A-1-d-Y | 254.4 | 270.1 | 0.942 |
| A-0-s-Y | 238.0 | 255.2 | 0.933 |
| A-1-s-Y | 245.7 | 261.1 | 0.941 |
| B-0-d-Y | 804.0 | 851.2 | 0.945 |
| B-1-d-Y | 811.6 | 851.6 | 0.953 |
| | | Mean value | 0.948 |

**Table 13.** Summary of the reduction factors $\chi_i$ and $\chi_{n,\,N-M}$.

| **Joint** | **No axial load** | **Axial load** |
|---|---|---|
| Interior | $\chi_i = 1.0$ | $\chi_i = 1.0$ |
| | $\chi_{n,\,N-M} = 1.0$ | $\chi_{n,\,N-M} = 0.95$ |
| Exterior | $\chi_i = 0.95$ | $\chi_i = 0.95$ |
| | $\chi_{n,\,N-M} = 1.0$ | $\chi_{n,\,N-M} = 0.95$ |

This being, all the terms in Eq. (7) are known and the value of $V_{y,\,Rk,\,compl}$ can be analytically predicted.

## 5.2. CONTRIBUTION $\Delta V_{Y,\,RK,\,COMPL}$ OF THE SE

From the parametric study, it was concluded that, beyond the yielding of the CWP, extra shear forces are transferred to the SE until a collapse mechanism develops, this collapse mechanism being activated regardless the presence or otherwise of transverse column web stiffeners. Therefore, the collapse mechanisms have been studied for each joint configuration in order to quantify the contribution $\Delta V_{y,\,Rk,\,compl}$ of the SE. For unstiffened joints, the collapse mechanism consists of the formation of four plastic hinges in the column flanges (see Table 14), thus leading to Eq. (12). For stiffened joints, two to four additional hinges are required in order for the collapse mechanism to develop (see Table 14). These additional plastic hinges are located either in the transverse column

*Published in : Journal of Constructional Steel Research (2022), vol. 189, 107099*
*DOI: 10.1016/j.jcsr.2021.107099*
*Status : Postprint (Author's version)*

web stiffeners or in the beam(s) flanges, the plastic collapse mechanism which actually develops being the one requiring the minimum energy, as stated by Eq. (13).

**Table 14.** List of all possible plastic collapse mechanisms for (un-)stiffened interior and exterior joints.

| | Unstiffened configurations | Stiffened configurations | |
|---|---|---|---|
| Interior joints | 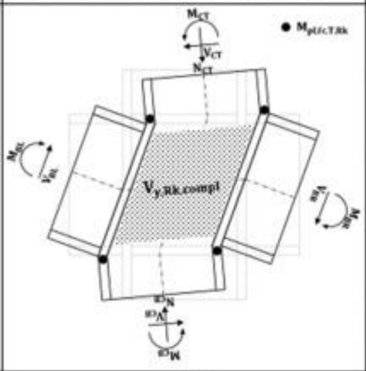 | 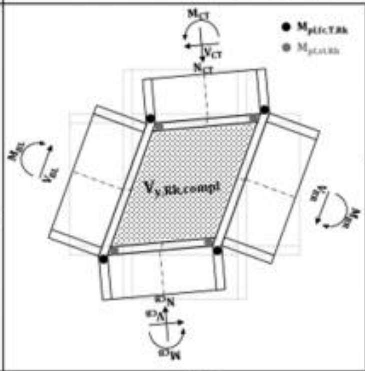 | 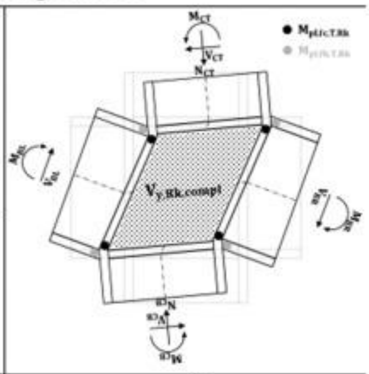 |
| Exterior joints | 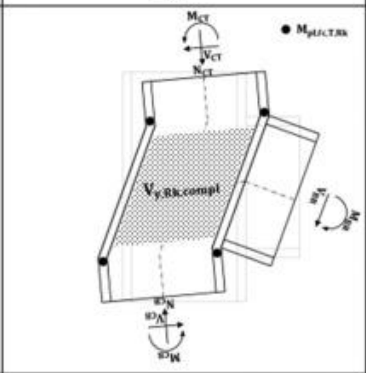 | 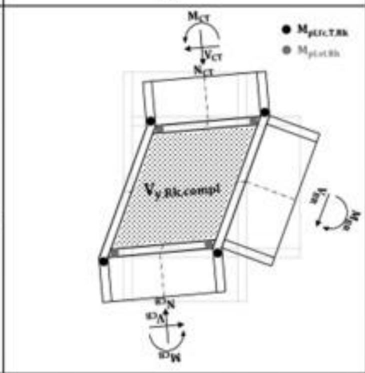 | 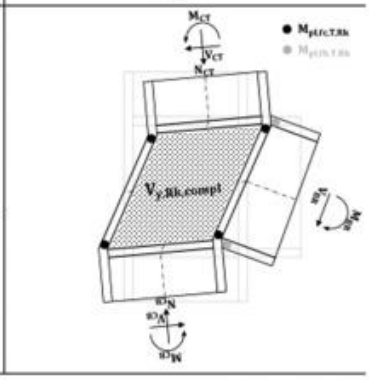 |
| $\Delta V_{y,Rk,compl}$ | $4 \cdot \frac{M_{pl,fc,T,Rk}}{d_b}$ (1) | $\begin{cases} \frac{4 \cdot M_{pl,fc,T,Rk} + 4 \cdot min(M_{pl,fb,T,Rk}; M_{pl,st,Rk})}{d_b} & int. joints \\ \frac{4 \cdot M_{pl,fc,T,Rk} + min(2 \cdot M_{pl,fb,T,Rk}; 4 \cdot M_{pl,st,Rk})}{d_b} & ext. joints \end{cases}$ (2) | |

In Eq. (12) and Eq. (13), $d_b$ is the lever arm between the centres of tension and compression (i.e. the height of the PZ, see Fig. 1), $M_{pl, fc, T, Rk}$, $M_{pl, fb, T, Rk}$ and $M_{pl, st, Rk}$ are the characteristic plastic moments of a T-shaped column flange including the root fillets region, of a T-shaped beam flange including the root fillets region and of a rectangular transverse column web stiffener, respectively. In addition, $M_{pl, fc, T, Rk}$, $M_{pl, fb, T, Rk}$ and $M_{pl, st, Rk}$ are reduced plastic moments as the column flanges, beam flanges and transverse column web stiffeners also carry an axial load. The vertical axial load in the column flanges comes from the column bending moment $M_C$ and from the axial load $N$ in the column, if any (see Fig. 3 and Fig. 4). The horizontal axial load in the beam flanges/the transverse column web stiffeners comes from the beam bending moment $M_B$ only as the beams were assumed not to carry any axial load in the scope of this article (i.e. $N_B = 0$ in Fig. 3 and Fig. 4).

For sake of clarity, some reasonable assumptions were made regarding the complex phenomena involved in the resistance $\Delta V_{y, Rk, compl}$ of the SE. These assumptions are listed herebelow and were proven to have no significant influence on the 28 numerical results considered in the present article. This is due to the fact that the contribution $\Delta V_{y, Rk, compl}$ of the SE rarely exceeds 25%–30% of the total shear resistance $V_{PZ, Rk, compl}$ of the PZ.

Published in : Journal of Constructional Steel Research (2022), vol. 189, 107099
DOI: 10.1016/j.jcsr.2021.107099
Status : Postprint (Author's version)

- Firstly, the plastic moment of a T-shaped beam flange including the root fillets region under M-N can be reasonably substituted by the plastic moment of a rectangular beam flange excluding the root fillets region under M only, i.e. $M_{pl,\,fb,\,T,\,Rk}$ can be replaced by $M^{*}_{pl,\,fb,\,Rk}$ in Eq. (13);
- Similarly, in the absence of any axial load $N_B$ in the beam(s), it is a reasonable assumption to neglect the M-N interaction in the derivation of the plastic moment of the stiffeners, i.e. $M_{pl,\,st,\,Rk}$ can be replaced by $M^{*}_{pl,\,st,\,Rk}$ in Eq. (13);
- Finally, in the absence of any axial load $N$ in the column, it is a reasonable assumption to neglect the M-N interaction in the derivation of the plastic moment of the T-shaped column flanges, i.e. $M_{pl,\,fc,\,T,\,Rk}$ can be replaced by $M^{*}_{pl,\,fc,\,T,\,Rk}$ in Eq. (12) and Eq. (13). Indeed, it was shown in the numerical simulations that the axial load coming from the $M_C$ bending moment is usually significantly smaller than the axial strength of the column flanges.

However, in the presence of a strong axial load $N$ in the column (see Fig. 3 and Fig. 4), the M-N interaction in the column flanges may no longer be neglected, as it was shown, in the parametric study, that the column flanges carry most of the axial load upon yielding of the CWP. This is expressed through Eq. (14) for a T-shaped column flange, where $\Delta\chi_{n,\,N\text{–}M}$ is a reduction factor accounting for the M-N interaction and $M^{*}_{pl,\,fc,\,T,\,Rk}$ is the characteristic plastic moment of a T-shaped column flange in the absence of any axial load in the column:

$$M_{pl,fc,T,Rk} = \Delta\chi_{n,N-M} \cdot M^{*}_{pl,fc,T,Rk} \quad (14)$$

In order to derive the parameter $\Delta\chi_{n,\,N\text{–}M}$, the M-N interaction curves of the T-shaped column flanges have been derived for the HEB160, HEB300 and HEB340 column profiles considered in this article. These M-N interaction curves are reported in Fig. 10.

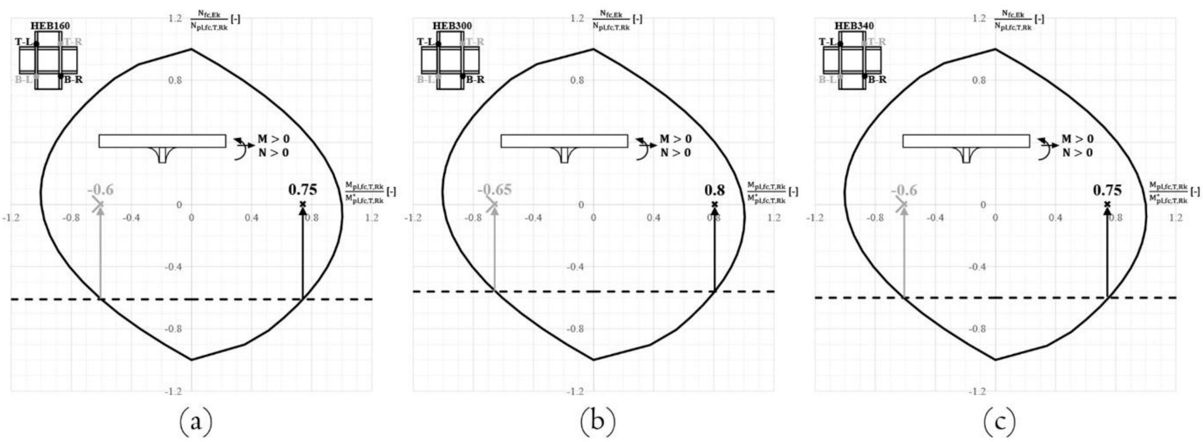


**Fig. 10.** M-N interaction curves of a T-shaped column flange: (a) HEB160, (b) HEB300 and (c) HEB340.

Knowing the level of the axial load in the column flanges (i.e. $\frac{0.25 \cdot N_{pl,c,Rk}}{N_{pl,fc,T,Rk}}$, Npl, c, Rk and Npl, fc, T, Rk being the axial strengths of the column cross-section and of a T-shaped column flange, respectively), the reduction factor Δχn, N−M associated to each plastic hinge forming in the column flanges can be easily obtained from Fig. 10. In Fig. 10, difference is made between the hinges forming in the top left (T-L) and bottom right (B-R) corners of the PZ under a positive bending moment, and the hinges

*Published in : Journal of Constructional Steel Research (2022), vol. 189, 107099*
*DOI: 10.1016/j.jcsr.2021.107099*
*Status : Postprint (Author's version)*

forming in the top right (T-R) and bottom left (B-L) corners of the PZ under a negative bending moment.

## 5.3. VALIDATION

Based on the results obtained from 5.1 Contribution, 5.2 Contribution, one can derive the $V_{y,\,Rk,\,compl}$ contribution for every single configuration, using Eq. (7), and sum it up with its corresponding $\Delta V_{y,\,Rk,\,compl}$ contribution, using Eq. (12) and Eq. (13). The result provides the total plastic shear resistance $V_{PZ,\,Rk,\,compl}$ (see Eq. (6)) for the new complex analytical model proposed in this article. These results are given in Table 15 where they are compared to the $V_{PZ,\,Rk,\,num}$ values, i.e. the numerical estimations of the plastic shear resistance of the PZ provided by the Abaqus© software (see Table 9). These latter have been extracted from the numerical $V-\gamma$ curves using the graphical method of Jaspart (see Section 3), i.e. the $V_{PZ,\,Rk,\,num}$ values are defined at the intersection between the y-axis and the line tangent to the residual post-plastic stiffness (see the red dotted lines in Fig. 7(a) and (b)). This residual post-plastic stiffness comes from the consideration in the Abaqus© software of the true stress-strain curve of the elastic-perfectly plastic steel material. The relative errors $E$ between the numerical values $V_{PZ,\,Rk,\,num}$ and the analytical predictions $V_{PZ,\,Rk,\,compl}$ are also reported in Table 15. They allow characterizing the level of accuracy of the analytical model, using the same categories and colour code as for Table 3, i.e. high accuracy category if $|E| \leq 5\%$ (see the light green boxes in Table 15), moderate accuracy category if $5\,\% < |E| \leq 10\%$ (see the light orange boxes in Table 15) and low accuracy category if $|E| > 10\%$ (see the light red boxes in Table 15).

**Table 15.** Comparison between $V_{PZ,\,Rk,\,compl}$ and $V_{PZ,\,Rk,\,num}$.

| Configurations | Category I X="d", Y="/" | | | Category II X="s", Y="/" | | | Category III X="d", Y="0.5N$_{pl}$" | | | Category IV X="s", Y="0.5N$_{pl}$" | | |
|---|---|---|---|---|---|---|---|---|---|---|---|---|
| | $V_{PZ,Rk,num}$ [kN] | $V_{PZ,Rk,compl}$ [kN] | $E$ [%] | $V_{PZ,Rk,num}$ [kN] | $V_{PZ,Rk,compl}$ [kN] | $E$ [%] | $V_{PZ,Rk,num}$ [kN] | $V_{PZ,Rk,compl}$ [kN] | $E$ [%] | $V_{PZ,Rk,num}$ [kN] | $V_{PZ,Rk,compl}$ [kN] | $E$ [%] |
| NR4-0-X-Y | 292 | 304.4 | 2.96 | 281.9 | 291.2 | 2.13 | 278.3 | 277.9 | -1.92 | 259.5 | 264.8 | -0.04 |
| NR4-I-X-Y | 321.2 | 328.0 | 0.90 | 300 | 303.0 | -1.05 | 303.3 | 301.5 | -2.65 | 280 | 276.6 | -4.07 |
| NR16-0-X-Y | 798.2 | 808.5 | 0.71 | 760 | 773.9 | 1.22 | 773.9 | 741.5 | -4.64 | 699.1 | 706.9 | 0.36 |
| NR16-I-X-Y | 1027.8 | 985.4 | -3.27 | 892.2 | 862.3 | -3.93 | 977.4 | 918.4 | -5.05 | 847.1 | 795.3 | -6.83 |
| A-0-X-Y | 334 | 331.9 | -1.24 | 315 | 318.8 | 0.65 | 310 | 296.7 | -5.08 | 283.3 | 283.5 | -1.02 |
| A-I-X-Y | 352.9 | 345.3 | -1.64 | 330 | 325.5 | -4.03 | 325 | 310.1 | -3.77 | 304.7 | 290.2 | -3.86 |
| B-0-X-Y | 1060 | 1083.3 | 1.98 | | | | 983.3 | 968.6 | -1.73 | | | |
| B-I-X-Y | 1080 | 1104.4 | 0.79 | | | | 1005.5 | 989.7 | -1.97 | | | |

Based on these values, the following conclusions can be drawn regarding the performances of the complex analytical model:

- Generally speaking, the proposed complex analytical model seems to work well, as it features a high level of accuracy for 25 out of the 28 simulations and a moderate to high level of accuracy for the 3 remaining simulations;

*Published in : Journal of Constructional Steel Research (2022), vol. 189, 107099*
*DOI: 10.1016/j.jcsr.2021.107099*
*Status : Postprint (Author's version)*

- For the non-axially loaded joints (i.e. the categories I and II in Table 15), the relative errors $E$ oscillate between −5% and 5%;
- For the axially loaded joints (i.e. categories III and IV in Table 15), the model is a bit more conservative, all the relative errors $E$ being negative.

Finally, the proposed complex analytical model also shows good performance (i.e. high level of accuracy) when compared to the 8 experimental results introduced in Section 3 (see the model of Corman in Fig. 5 and Table 3).

# 6. Towards a simplified analytical model for practice

## 6.1. CONTRIBUTION $V_{Y,RK,SIMPL}$ OF THE CWP

In order to simplify the derivation of the contribution $V_{y,Rk,compl}$ of the CWP (see Eq. (7)), it is proposed to replace, in the derivation of $V^*_{y,Rk,compl}$, the complex shear stress distribution over $A_{VC}$, defined in Fig. 9(b), by a simpler one, which is easier to integrate. This one is defined in Fig. 9(c) and consists of a uniform shear stress distribution over the whole depth of the column. In order to assess the validity of this assumption, the ratio $V^*_{y,Rk,simpl}/V^*_{y,Rk,compl}$ was plotted against the flange thickness $t_{fc}$ for all the relevant American W-profiles and European HE-profiles, i.e. those characterized by $0.55 \le t_{wc}/t_{fc} \le 0.62$ (see Table 16). In Table 16, difference is made between the profiles characterized by thin flanges, i.e. $t_{fc} \le 40mm$, or thick flanges, i.e. $t_{fc} > 40mm$. The following observations can be made from Table 16:

- For the American "thin flanges" W-profiles, the ratio $V^*_{y,Rk,simpl}/V^*_{y,Rk,compl}$ oscillates around 1.05. Therefore, it is proposed to use $V^*_{y,Rk,simpl}/0.95$ as a good approximation of $V^*_{y,Rk,compl}$.
- By contrast, for the "thick flanges" W-profiles, the ratio $V^*_{y,Rk,simpl}/V^*_{y,Rk,compl}$ significantly diverges from 1.0 with increasing flange thickness. This observation is in line with the conclusion drawn in [7,11,13]. Thus, it is suggested, for this range of W-profiles, to keep the complex definition of $V^*_{y,Rk,compl}$.
- For the European "thin flanges" HE-profiles, the ratio oscillates around 1.0. Therefore, $V^*_{y,Rk,simpl}$ may be used instead of $V^*_{y,Rk,compl}$.
- Finally, it can be observed that very few European HE-profiles are characterized by flanges larger than 40 mm. For these particular profiles, the ratio $V^*_{y,Rk,simpl}/V^*_{y,Rk,compl}$ oscillates around 1.05. Therefore, it is proposed to use $V^*_{y,Rk,simpl}/0.95$ as a good approximation of $V^*_{y,Rk,compl}$, similarly to the American "thin flanges" W-profiles.

*Published in : Journal of Constructional Steel Research (2022), vol. 189, 107099*
*DOI: 10.1016/j.jcsr.2021.107099*
*Status : Postprint (Author's version)*

**Table 16.** Comparison between $V^*_{y,Rk,simpl}$ and $V^*_{y,Rk,compl}$ for the relevant US W-profiles and EU HE-profiles.

| | $t_{fc} \leq 40mm$ | $t_{fc} > 40mm$ |
|---|---|---|
| US W-profiles | 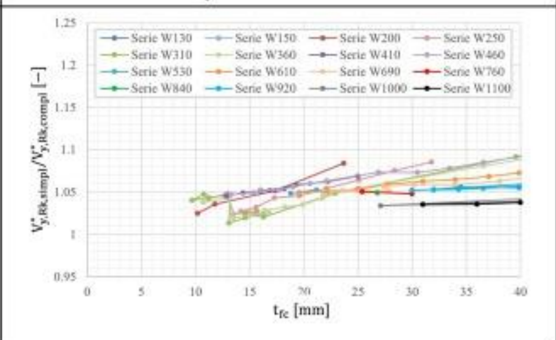 | 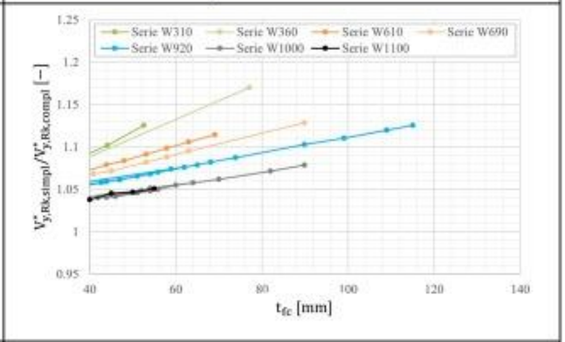 |
| EU HE-profiles | 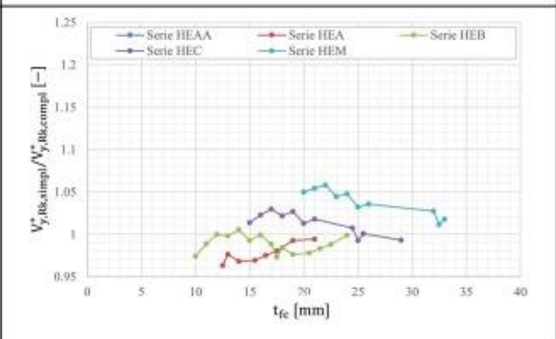 | 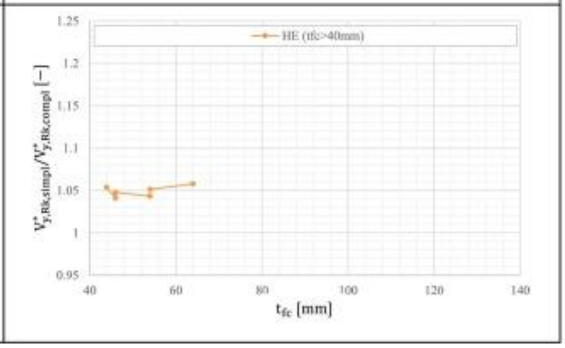 |

Based on these observations, Eq. (7) can be substituted by Eq. (15):

$$V_{y,Rk,simpl} = \chi_{n,N-M} \cdot \chi_i \cdot \frac{V^*_{y,Rk,simpl}}{\eta} \quad (15)$$

where:

$\chi_{n,N-M}$, $\chi_i$: stress interaction factors defined in Table 13

$$V^*_{y,Rk,simpl} = \begin{cases} t_{wc} \cdot h_c \cdot \tau_y \text{for all EU HE-profiles an US "thin flanges" W-profiles} \\ V^*_{y,Rk,compl} \text{for US "thick flanges" W-profiles} \end{cases}$$

$$\eta = \begin{cases} 1.0 \text{for EU "thin flanges" HE-profiles} \\ 0.95 \text{for EU "thick flanges" HE-profiles and US "thin flanges" W-profiles} \end{cases}$$

## 6.2. CONTRIBUTION $\Delta V_{Y,RK,SIMPL}$ OF THE SE

Regarding the derivation of the contribution $\Delta V_{y,Rk,compl}$ of the SE, two simplifications are proposed. The first one consists in replacing, in Eq. (12) and Eq. (13), the plastic moment of a T-shaped column flange, i.e. $M_{pl,fc,T,Rk}$, by the plastic moment of a rectangular column flange, i.e. $M_{pl,fc,Rk}$. Therefore, Eq. (14) may be replaced by Eq. (16):

$$M_{pl,fc,Rk} = \Delta\chi_{n,N-M} \cdot M^*_{pl,fc,Rk} \quad (16)$$

This first assumption tends to decrease the contribution $\Delta V_{y,Rk,simpl}$ with respect to $\Delta V_{y,Rk,compl}$. As a counterpart, it is proposed to neglect the M-N interaction in the derivation of $M_{pl,fc,Rk}$, i.e. $\Delta\chi_{n,N-M} = 1.0$ in Eq. (16). In total, these two assumptions are assumed to compensate each other in the case of axially-loaded joints but will lead to conservative predictions in the case of non-axially loaded joints.

*Published in : Journal of Constructional Steel Research (2022), vol. 189, 107099*
*DOI: 10.1016/j.jcsr.2021.107099*
*Status : Postprint (Author's version)*

## 6.3. VALIDATION

Based on the simplifications proposed in 6.1 Contribution, 6.2 Contribution, one can derive the plastic shear resistance $V_{PZ,\ Rk,\ simpl}$ for the 28 joints considered in this article. The results are summarized in Table 17 and Table 18 for non-axially loaded joints and axially loaded joints, respectively. In Table 17 and Table 18 are also reported the results provided by the European design code (i.e. $V_{PZ, Rk, EU}$, see Eq. (3)) and the American design code (i.e. $V_{PZ, Rk, US}$, see Eq. (5)). Once again, the relative errors $E$ between the numerical values $V_{PZ,\ Rk,\ num}$ (coming from Table 15) and the analytical predictions (i.e. $V_{PZ,\ Rk,\ simpl}$, $V_{PZ,\ Rk,\ EU}$ and $V_{PZ,\ Rk,\ US}$) have been computed and classified into three main categories, namely the high accuracy category if $|E| \leq 5\%$ (see the light green boxes in Table 17 and Table 18), the moderate accuracy category if $5\ \% < |E| \leq 10\%$ (see the light orange boxes in Table 17 and Table 18) and the low accuracy category if $|E| > 10\%$ (see the light red boxes in Table 17 and Table 18). Based on these values, the following conclusions can be drawn regarding the performances of the analytical models:

- For axially loaded joints (see Table 18), the proposed simplified model seems to work well, as it features a high level of accuracy for 11 out of the 14 numerical simulations and a moderate level of accuracy for the 3 remaining simulations.
- For the non-axially loaded joints (see Table 17), as expected, the results are a bit more conservative, with 50% belonging to the moderate accuracy category while the other 50% belong to the high accuracy category.
- In addition, it can be noticed that (almost) all the relative errors $E$ are negative, which means that the simplified analytical model remains on the safe side.
- By contrast, both EU and US models show poor performances in the case of axially loaded joints (see Table 18), displaying a low level of accuracy for 11 and 10 out of the 14 axially loaded joints, respectively.
- For the non-axially loaded joints (see Table 17), these models perform a bit better with 7 and 3 poorly accurate predictions left among the 14 analytical predictions, respectively.
- Finally, almost all the relative errors $E$ associated to the EU and US models are positive, which means that these models tend to provide unsafe estimates of the actual plastic shear resistance of the PZ.

*Published in : Journal of Constructional Steel Research (2022), vol. 189, 107099*
*DOI: 10.1016/j.jcsr.2021.107099*
*Status : Postprint (Author's version)*

**Table 17.** Comparison between $V_{PZ,\,Rk,\,simpl}$, $V_{PZ,\,Rk,\,EU}$ and $V_{PZ,\,Rk,\,US}$ for the non-axially loaded joints.

| Configurations | Category III X="d", Y="/" | | | | | | Category IV X="s", Y="/" | | | | | |
|---|---|---|---|---|---|---|---|---|---|---|---|---|
| | $V_{PZ,Rk,simpl}$ [kN] | $E$ [%] | $V_{PZ,Rk,EU}$ [kN] | $E$ [%] | $V_{PZ,Rk,US}$ [kN] | $E$ [%] | $V_{PZ,Rk,simpl}$ [kN] | $E$ [%] | $V_{PZ,Rk,EU}$ [kN] | $E$ [%] | $V_{PZ,Rk,US}$ [kN] | $E$ [%] |
| NR4-0-X-Y | 292.5 | 0.17 | 324.5 | 11.13 | 312.7 | 7.10 | 279.4 | -0.90 | 324.5 | 15.11 | 312.7 | 10.94 |
| NR4-1-X-Y | 316.1 | -1.60 | 354.6 | 10.41 | 312.7 | -2.64 | 291.2 | -2.95 | 354.6 | 18.21 | 312.7 | 4.24 |
| NR16-0-X-Y | 757.8 | -5.06 | 874.9 | 9.61 | 809.5 | 1.42 | 724.0 | -4.74 | 874.9 | 15.11 | 809.5 | 6.52 |
| NR16-1-X-Y | 934.7 | -9.06 | 956.3 | -6.95 | 809.5 | -21.23 | 812.5 | -8.94 | 956.3 | 7.19 | 809.5 | -9.26 |
| A-0-X-Y | 312.5 | -6.44 | 324.5 | -2.85 | 345.5 | 3.44 | 299.4 | -4.97 | 324.5 | 3.02 | 345.5 | 9.68 |
| A-1-X-Y | 325.9 | -7.66 | 374.6 | 6.16 | 345.5 | -2.10 | 306.1 | -7.26 | 374.6 | 13.52 | 345.5 | 4.69 |
| B-0-X-Y | 1006.4 | -5.06 | 1034.6 | -2.39 | 1120.5 | 5.70 | | | | | | |
| B-1-X-Y | 1027.5 | -4.86 | 1204.8 | 11.55 | 1120.5 | 3.75 | | | | | | |

**Table 18.** Comparison between $V_{PZ,\,Rk,\,simpl}$, $V_{PZ,\,Rk,\,EU}$ and $V_{PZ,\,Rk,\,US}$ for the axially loaded joints.

| Configurations | Category III X="d", Y="0.5N$_{pl}$" | | | | | | Category IV X="s", Y="0.5N$_{pl}$" | | | | | |
|---|---|---|---|---|---|---|---|---|---|---|---|---|
| | $V_{PZ,Rk,simpl}$ [kN] | $E$ [%] | $V_{PZ,Rk,EU}$ [kN] | $E$ [%] | $V_{PZ,Rk,US}$ [kN] | $E$ [%] | $V_{PZ,Rk,simpl}$ [kN] | $E$ [%] | $V_{PZ,Rk,EU}$ [kN] | $E$ [%] | $V_{PZ,Rk,US}$ [kN] | $E$ [%] |
| NR4-0-X-Y | 279.4 | 0.38 | 324.5 | 16.60 | 312.7 | 12.37 | 266.3 | 2.60 | 324.5 | 25.05 | 312.7 | 20.51 |
| NR4-1-X-Y | 303.0 | -0.11 | 354.6 | 16.93 | 312.7 | 3.11 | 278.0 | -0.70 | 354.6 | 26.66 | 312.7 | 11.69 |
| NR16-0-X-Y | 724.0 | -6.45 | 874.9 | 13.05 | 809.5 | 4.61 | 690.2 | -1.28 | 874.9 | 25.14 | 809.5 | 15.80 |
| NR16-1-X-Y | 900.9 | -7.83 | 956.3 | -2.16 | 809.5 | -17.17 | 778.6 | -8.08 | 956.3 | 12.89 | 809.5 | -4.43 |
| A-0-X-Y | 299.4 | -3.43 | 324.5 | 4.68 | 345.5 | 11.44 | 286.2 | 1.04 | 324.5 | 14.54 | 345.5 | 21.95 |
| A-1-X-Y | 312.7 | -3.77 | 374.6 | 15.27 | 345.5 | 6.30 | 292.9 | -3.86 | 374.6 | 22.95 | 345.5 | 13.38 |
| B-0-X-Y | 964.6 | -1.90 | 1034.6 | 5.22 | 1120.5 | 13.95 | | | | | | |
| B-1-X-Y | 985.7 | -1.97 | 1204.8 | 19.82 | 1120.5 | 11.43 | | | | | | |

# 7. Conclusions and perspectives

In conclusion, this article proposes a new promising analytical model for the prediction of the plastic shear resistance of the PZ in welded steel beam-to-column joints under monotonic loading. This model has been developed based on the understanding of the physical phenomena governing the plastic shear resistance of the PZ. This understanding has been gained through the analysis of the numerical results coming from the extensive parametric study carried out with the Abaqus© software. This way, the newly proposed model features the following characteristics:

- it accounts for both contributions $V_{y,\,Rk,\,compl}$ and $\Delta V_{y,\,Rk,\,compl}$ of the CWP and the SE, separately;

- the contribution $V_{y,\,Rk,\,compl}$ of the CWP has been developed based on the analysis and the integration of the actual shear stress distribution in the CWP at yielding;
- the contribution $\Delta V_{y,\,Rk,\,compl}$ of the SE has been derived based on the analysis of the collapse mechanism which actually develops within the SE;
- the $\tau - \sigma_i$ interaction has been taken into account in the contribution $V_{y,\,Rk,\,compl}$ only, through the use of a reduction factor $\chi_i$. This interaction has to be accounted for in the case of exterior joint configurations only;
- the $\tau - \sigma_{n,\,N-M}$ interaction has been taken into account in both contributions $V_{y,\,Rk,\,compl}$ and $\Delta V_{y,\,Rk,\,compl}$ through the use of two reduction factors, $\chi_{n,\,N-M}$ and $\Delta\chi_{n,\,N-M}$, eventhough it was observed that most of the axial load is carried by the column flanges. This interaction has to be accounted for in the presence of an axial load in the column only.

The so-developed analytical model has proven to work well through comparisons with numerical and experimental results. The authors recommend the use of this complex model for scientific purposes. In addition, a simplified version of this model has also been proposed in view of its integration in modern design codes. Despite being more conservative, this simplified model shows good performance, especially for axially-loaded joints, and outperforms current EN 1993-1-8 and AISC predictive models.

Following steps include the validation of the complex analytical model for column profiles characterized by different web-to-flange thickness ratios than those considered in the present article (i.e. $t_{wc}/t_{fc} \notin [0.55 - 0.62]$), as well as for higher axial loads (i.e. $N > 0.5N_{pl}$). This model should then be extended to PZ in bolted joints. Finally, perspectives regarding the simplified analytical model include a better consideration of the axial load by the model and the derivation of a simplified analytical formula for the stocky column profiles characterized by thick column flanges (i.e. $t_{fc} > 40mm$).

# Declaration of Competing Interest

The authors declare that they have no known competing financial interests or personal relationships that could have appeared to influence the work reported in this paper.

# Acknowledgment

This scientific publication is supported by the Wallonia-Brussels Federation within the framework of a FRIA grant.

*Published in : Journal of Constructional Steel Research (2022), vol. 189, 107099*
*DOI: 10.1016/j.jcsr.2021.107099*
*Status : Postprint (Author's version)*

# References

[1] J.-P. Jaspart, K. Weynand, Design of Joints in Steel and Composite Structures. Berlin, 2016.

[2] R. Maquoi, J.P. Jaspart, Load-introduction resistance of column webs in strong Axis beam-to-column joints, in: Contact Loading and Local Effects in Thin-walled Plated and Shell Structures, 1992, pp. 204–211.

[3] J.S. Huang, D.J. Fielding, J.S. Huang, Shear in steel beam-to-column connections, Weld. Res. Suppl (1971) 313–326.

[4] H. Augusto, L. Simões da Silva, C. Rebelo, J.M. Castro, Characterization of web panel components in double-extended bolted end-plate steel joints, J. Constr. Steel Res. 133 (2017) 310–333, https://doi.org/10.1016/j.jcsr.2017.01.021.

[5] A. Corman, J.-P. Jaspart, J.-F. Demonceau, Resistance of the beam-to-column component column web panel in shear, Steel Constr. 12 (3) (2019), https://doi.org/10.1002/stco.201900020.

[6] G. Brandonisio, Il pannello nodale nei collegamenti trave-colonna saldati (Msc thesis, in Italian), University of Naples (Italy), 2004.

[7] H. Krawinkler, Shear in beam-column joints in seismic design of steel frames, Eng. J. 15 (1978) 88–91 [Online]. Available: https://www.aisc.org/Shear-in-Beam-Column-Joints-in-Seismic-Design-of-Steel-Frames.

[8] L.-W. Lu, S.-J. Wang, S.-J. Lee, Cyclic behaviour of steel and composite joints with panel zone deformation, in: Proceedings of 9th World Conference on Earthquake Engineering, Tokyo-Kyoto, Japan, 1988, pp. 701–706.

[9] J.-P. Jaspart, Etude de la semi-rigidité des nœuds poutre-colonne et son influence sur la résistance et la stabilité des ossatures en acier (PhD thesis, in French), University of Liège (Belgium) (1991).

[10] K.C. Lin, K.C. Tsai, S.L. Kong, S.H. Hsien, Effects of Panel Zone Deformations on Cyclic Performance of Welded Moment Connections, 2000.

[11] K.D. Kim, M.D. Engelhardt, Monotonic and cyclic loading models for panel zones in steel moment frames 58, 2002, pp. 5–8.

[12] D.W. Kim, C. Blaney, C.M. Uang, Panel zone deformation capacity as affected by weld fracture at column kinking location, Eng. J. 52 (1) (2015) 27–46.

[13] A. Skiadopoulos, A. Elkady, D.G. Lignos, Proposed Panel Zone Model for Seismic Design of Steel Moment-Resisting Frames, J. Struct. Eng. 147 (4) (2021) 04021006, https://doi.org/10.1061/(asce)st.1943-541x.0002935.

[14] European Committee for Standardization, "NBN EN 1993-1-1 – Eurocode 3 : Design of steel structures – Part 1–1 : General rules and rules for buildings," Brussels, 2005.

[15] European Committee for Standardization, NBN EN 1993-1-8 – Eurocode 3: Design of Steel Structures – Part 1–8: Design of Joints (English Version). Brussels, 2005.

[16] American Institute of Steel Construction, Specification for Structural Steel Buildings. Chicago, 2016.

[17] H. Klein. Das elastisch - plastische Last-Verformungsverhalten M-theta steifenloser, geschweisster Knoten für die Berechnung von Stahlrahmen mit HEB-Stützen (PhD thesis, in German), University of Innsbruck, Austria, 1985.

[18] G. Brandonisio, A. De Luca, E. Mele, Shear strength of panel zone in beam-tocolumn connections, J. Constr. Steel Res. 71 (2012) 129–142, https://doi.org/10.1016/j.jcsr.2011.11.004.

[19] P. Baliozoglou. Investigation of external thin-walled joints in steel frames with experimental, analytical and numerical methods (Msc thesis, in Greek), National Technical University of Athens, Greece, 2020.

[20] S. Jordão, L. Simões Da Silva, R. Simões, Behaviour of welded beam-to-column joints with beams of unequal depth, J. Constr. Steel Res. 91 (2013) 42–59, https://doi.org/10.1016/j.jcsr.2013.07.023.

[21] A.L. Ciutina, D. Dubina, Influence of column web stiffening on the seismic behaviour of beam-to-column joints, Stessa 2003 Behav. Steel Struct. Seism. Areas (2003) 269–275.

[22] D. Dubina, A. Ciutina, A. Stratan, Cyclic tests of double-sided beam-to-column joints, J. Struct. Eng. 127 (2) (2001) 129–136.

[23] M. Elflah, M. Theofanous, S. Dirar, H. Yuan, Behaviour of stainless steel beam-tocolumn joints — part 1: experimental investigation, J. Constr. Steel Res. 152 (2019) 183–193, https://doi.org/10.1016/j.jcsr.2018.02.040.

[24] P. Zanon, R. Zandonini, Experimental analysis of end plate connections, in: ProceedingState of the ArtWorkshop on Connections and the Behaviour of Strength and Design of Steel Structuress of a State-of-the-Art Workshop on Connections and the Behaviour, Strength and Design of Steel Structures, 1988, pp. 41–51.

[25] K. Weynand. Sicherheits-und Wirtsschaftlichkeitsuntersuchungen zur anwendung nachgiebiger anschlüsse im stahlbau (PhD thesis, in German), University of Aachen, Germany, 1997.

[26] SIMULIA, ABAQUS user's manual 6.14. http://130.149.89.49:2080/v6.14/, 2014.

[27] F. Frey, W. Atamaz Sibai, Numerical simulation of the behaviour up to collapse of two welded unstiffened one-side flange connections, in: Connections and the Behaviour, Strength and Design of Steel Structures, 1987, pp. 85–92.

[28] European Committee for Standardization, NBN EN 1993-1-14 – Eurocode 3: Design of steel structures – Part 1-14: Design assisted by finite element analysis (English version). Brussels, 2021.

[29] X. Yun, L. Gardner, Stress-strain curves for hot-rolled steels, J. Constr. Steel Res. 133 (June) (2017) 36–46, https://doi.org/10.1016/j.jcsr.2017.01.024.

*Published in : Journal of Constructional Steel Research (2022), vol. 189, 107099*
*DOI: 10.1016/j.jcsr.2021.107099*
*Status : Postprint (Author's version)*

[30] H. Namba, M. Tabuchi, T. Tanaka, Evaluation for Restoring Force Characteristic of Joint Panels with Various Cross Sections (in Japanese), Steel Constr. Eng. 11 (42) (2004).

[31] F. Rahiminia, H. Namba, Joint panel in steel moment connections, Part 1: Experimental tests results, J. Constr. Steel Res. 89 (2013) 272–283, https://doi.org/10.1016/j.jcsr.2013.07.002.

[32] B. Kato, W.F. Chen, M. Nakao, Effects of joint-panel shear deformation on frames, J. Constr. Steel Res. 10, no. C (1988) 269–320, https://doi.org/10.1016/0143-974X(88)90033-8.